Methane + neo-pentane system: VLE measurements, modeling of the phase diagram including solid phases

Marco Campestrini, Alain Valtz, Salem Hoceini, Paolo Stringari

Methane+neo-Pentane system: VLE measurements and modeling of the phase diagram including solid phases

Marco Campestrini*, Alain Valtz, Salem Hoceini, Paolo Stringari

MINES ParisTech, PSL Research University, CTP – Centre of Thermodynamics of Processes, 35 rue St Honoré 77300 Fontainebleau, France

* Corresponding author. Tel.: +33 (0)1 64 69 49 80. E-mail address: marco.campestrini@mines-paristech.fr

Abstract

New measurements of isothermal vapor-liquid equilibrium for the (CH_4+neoC_5H_{12}) system have been carried out using a static-analytic method for temperatures from 213 K up to 345 K and pressures up to 13 MPa. The method of Ungerer et al. has been used to extrapolate the VLE data to the critical-points region.

Measured VLE data have been compared with literature values and used for investigating the low-temperature phase equilibrium behavior of the system (temperatures lower than the triple-point temperature of neo-pentane down to 213 K) where literature SVE data and thermodynamic models are in partial disagreement.

Measured VLE data agree with literature VLE data and low-temperature VLE calculated from predictive models (PPR78 and PSRK EoSs). The new phase equilibrium measurements obtained at temperatures lower than the triple point temperature of neoC_5H_{12} have allowed solving the discrepancy between literature data and model predictions and determining the global phase diagram of the system following the van Konynenburg and Scott's and the Kohn and Luks' classifications.

Keywords: Methane, neo-Pentane, VLE, Solid phase, Global phase diagram

Nomenclature

LNG: Liquefied Natural Gas
EoS: Equation of State
CA: Classical Approach for the calculation of solid fugacity of a pure component
vle: saturation line of a pure component
sve: sublimation line of a pure component
sle: melting line of a pure component
sse: solid-solid transition line of neo-pentane
VLE: Vapor-Liquid Equilibrium of the mixture
VLLE: Vapor-Liquid-Liquid Equilibrium of the mixture
SVE: Solid-Vapor Equilibrium of the mixture
SLE: Solid-Liquid Equilibrium of the mixture
SLVE: Solid-Liquid-Vapor Equilibrium of the mixture
SSVE: Solid-Solid-Vapor Equilibrium of the mixture
SSLE: Solid-Solid-Liquid Equilibrium of the mixture
QP: Quadruple Point of the mixture
UCEP: Upper Critical End Point of the mixture
CP: Critical Point of the mixture
y: molar composition of the vapor phase
x: molar composition of the liquid phase
p: system pressure
T: system temperature
k_{ij}: binary interaction parameter
R: gas constant

Subscripts

1: related to methane
2: related to neo-pentane
α: crystal structure α of solid neo-pentane
β: crystal structure β of solid neo-pentane
c: critical-point properties
t: triple-point properties
μ, λ_1, λ_2: parameters of the extended scaling law

1. Introduction

The knowledge of phase equilibria and other thermodynamic properties of the streams involved in process train units (like acid gas removal and CO_2 capture units, dehydration and mercury removal units, fractionation and liquefaction trains) of LNG plants is mandatory for the proper and optimum design of the equipments toward the profitable and safe production of LNG. This applies for both the feed gas and the auxiliary fluids like refrigerants and would avoid the construction of undersized (loss of performances) or oversized (loss of profits) facilities. From the feed gas side, the design of cooling cycles and the liquefaction step requires mastering the thermodynamic properties of methane-rich fluid mixtures and the solubility limits of heavy components that may precipitate in these mixtures at the temperatures of the different unit operations of the process and of the storage and transport operations.

As a matter of fact, these solubility limits are often unknown and thus impact the profitability of the plants obliging gas companies to either realize more frequent maintenance operations or employ oversized purification units before the low-temperature cooling starts for avoiding technical issues related to solid deposition (reduced pipe diameters, coated walls of heat exchangers, altered flow rates and heat transfer efficiencies, increased pressure drops).

At the same time, some qualitative hypotheses on unknown solubility limits can be drawn by considering the properties of the heavy components. Indeed, as a general rule of thumb, the higher the triple-point temperature and the latent heat of melting of a potential solid former, the lower is the solubility of its solid phase in a solvent.

In that sense, neo-pentane (2,2-dimethylpropane) is of particular interest seeing that despite a high triple-point temperature (256.6 K, [1]) suggesting that the solubility of solid neo-pentane in methane should be low, its low enthalpy change upon melting (3.26 kJ/mol, [2]), compared to other common natural gas heavy-components, suggests a high degree of solubility.

In this paper, we present a deep investigation about the global phase equilibrium behavior of the methane+neo-pentane system in order to evaluate if neo-pentane has to be considered in the assessment of the crystallization risk in natural gas liquefaction processes.

This investigation relies on original low-temperature vapor-liquid equilibrium measurements carried out to settle the disagreement between the global phase equilibrium behavior of the mixture that can be inferred from equilibrium values available in the literature (section 2) and the one calculated by means of predictive models for the fluid phases when coupled with a solid-fugacity model (section 3).

2. Global phase equilibrium behavior from literature VLE, SVE, and SLVE data

Table 1 gathers some triple-point and critical-point properties and the acentric factors of methane and neo-pentane as taken from Ref. [3] and [1], respectively. The enthalpies of melting of methane and neo-pentane at the triple point (ΔH^{SLE}) have been taken from Ref. [4] and Ref. [2], respectively. The low-temperature phase equilibrium behavior (temperatures lower than the corresponding triple-point temperature) of both methane and neo-pentane are interested by some solid-solid transitions. At pressures of interest for industrial processes, solid-solid transition occurs at 20.4 K for methane [5], and at 140 K for neo-pentane [2]. Seeing that the present work has been limited to temperatures as low as 70 K, only properties related to the solid-solid transition of neo-pentane are gathered in Table 1.

Table 1. Acentric factor, triple-point and critical-point properties of methane and neo-pentane, solid-solid transition temperature and related enthalpy change of neo-pentane.
ω : acentric factor, [3,1]; T_t : triple-point temperature, [3,1]; p_t : triple-point pressure, [3,1]; ΔH^{SLE} : enthalpy change upon melting, [4,2]; T_c : critical-point temperature, [3,1]; p_c : critical-point pressure, [3,1]; T_t^* : solid-solid transition temperature of neo-pentane, [2]; ΔH^{SSE} : enthalpy change upon solid-solid transition of neo-pentane [2].

Component	ω	T_t K	p_t MPa	ΔH^{SLE} kJ/mol	T_c K	p_c MPa	T_t^* K	ΔH^{SSE} kJ/mol
CH_4	0.01142	90.694	0.011696	0.9414	190.56	4.5992		
$neoC_5H_{12}$	0.1961	256.6	0.035401	3.26	433.74	3.196	140.0	2.58

Table 2 presents the available literature values of Vapor-Liquid Equilibrium (VLE), Solid-Vapor Equilibrium (SVE), and Solid-Liquid-Vapor Equilibrium (SLVE) for the methane+neo-pentane system: the references, the kind of data, the number of data (N), the ranges of temperature, pressure, and composition, and the experimental methods are in the first, second, third, fourth, fifth, sixth, and last column of Table 2, respectively; S_2 refers to solid neo-pentane.

Table 2. Literature values for the binary system (1-x_2)CH_4+(x_2)neo-pentane

Ref.	Kind of data	*N*	Range of *T* K	Range of *p* MPa	x_2 range	y_2 range	Experimental method
[6]	VLE	18	344 – 411	2.1 – 12.0	0.40 – 0.95	0.18 – 0.72	Static
[7]	VLE	16	298.15	1.2 – 15.1	0.17 – 0.93	0.04 – 0.14	Static
	CP	1	298.15	15.2	0.155		
[8]	S_2VE	57	200 – 258	0.36 – 8.2		0.001 – 0.12	Dynamic
[9]	S_2LVE	3	100 – 123		0.01 – 0.026		Static

The VLE behavior of the system was investigated in 1971 by Prodany and Williams [6] and by Rogers and Prausnitz [7]. Literature VLE data are illustrated in Figure 1: filled circles are values at 344.24 K, 377.57 K, and 410.89 K reported in [6]; empty squares are values at 298.15 K reported in [7]; the filled square is the Critical Point (CP) of the system at 298.15 K reported in [7].

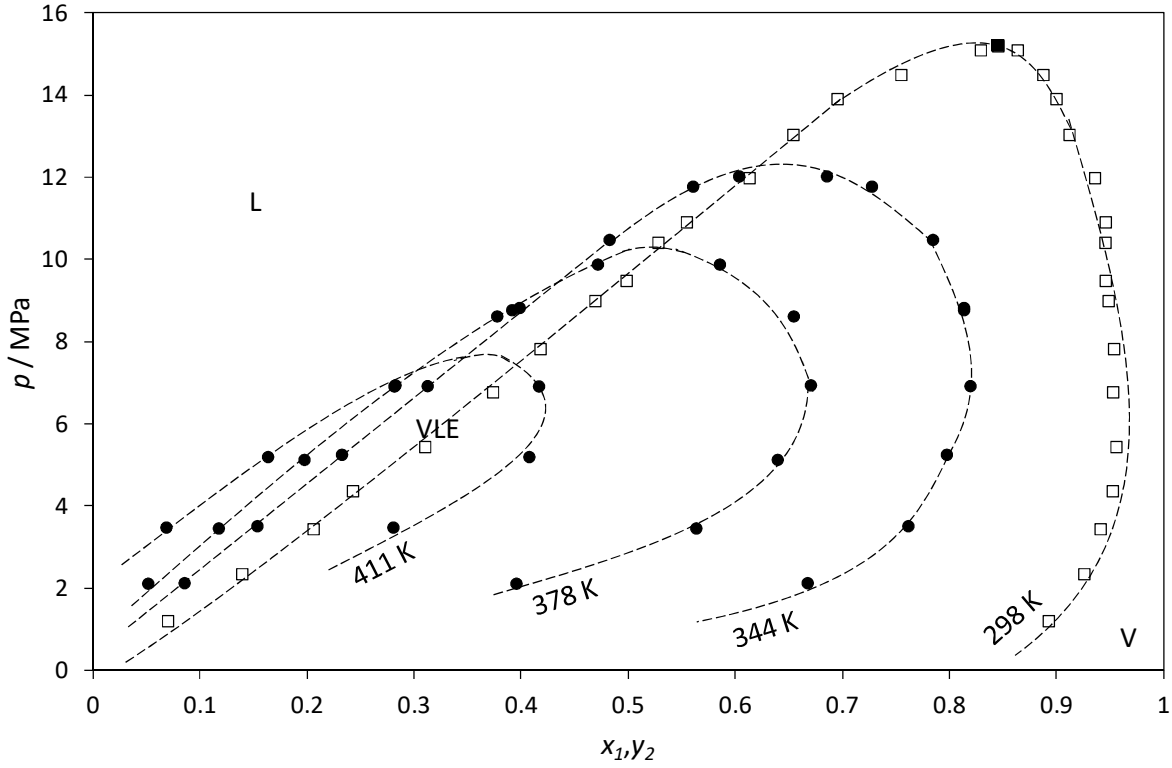

Figure 1. Literature VLE data from 298 K up to 411 K for the (1)CH_4+(2)neo-C_5H_{12} system.

Data: ● Ref. [6], □,■ Ref. [7]; – – : qualitative VLE compositions.

Baughman et al. in 1974 measured the SVE behavior of the system at temperatures between 199.99 K and 257.90 K by means of a single-pass flow method, [8]. Liquid neo-pentane was firstly fed at the top of a 7-trays equilibrium cell before decreasing the temperature down the target temperature lower than the triple-point of neo-pentane. A metering valve adjusted the rate of a flow of methane entering the bottom of the cell and flowing in a cross-flow pattern across the trays. The equilibrium vapor leaving the top of the cell was transferred to Gas Chromatographic Analysis (GCA). The neo-pentane compositions at SVE given in Ref. [8] are represented in Figure 2 by filled triangles, together with the vapor composition at VLE measured in 1971 (Refs. [6,7]).

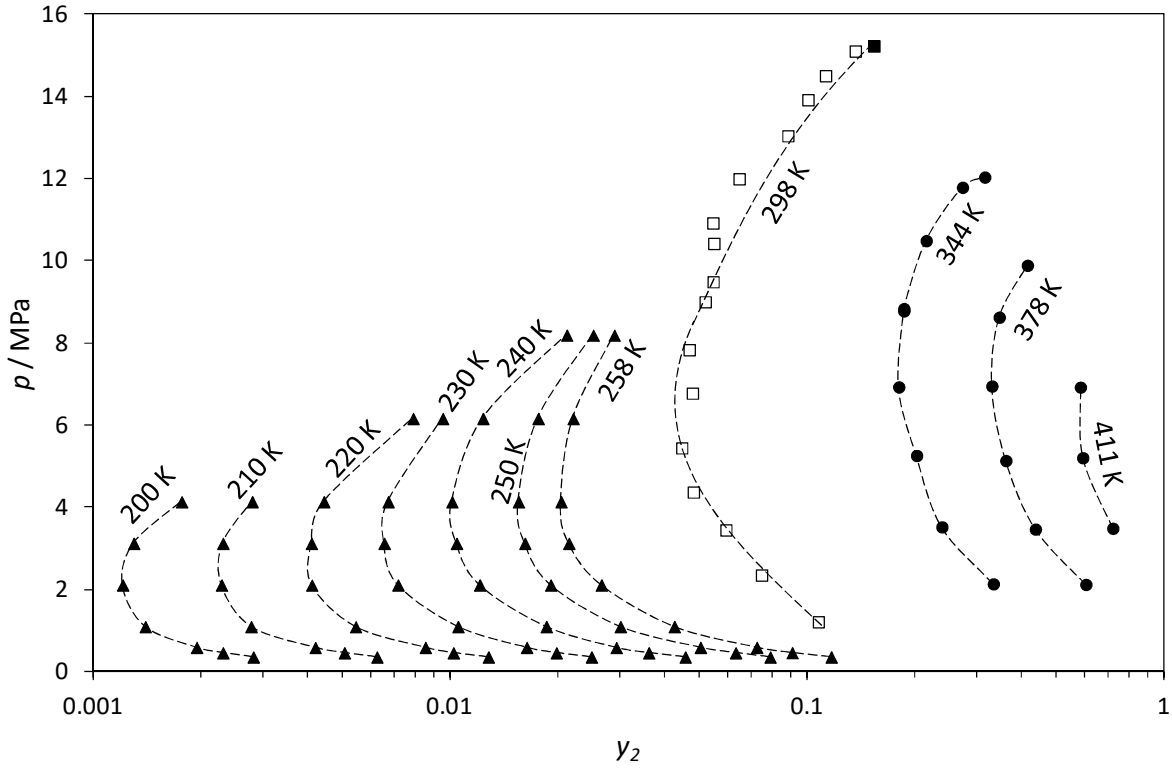

Figure 2. neo-pentane composition in the vapor phase at SVE from 200 K up to 258 K and at VLE from 298 K up to 411 K for the (1)CH_4+(2)neo-C_5H_{12} system.
VLE Data: ● Ref. [6], □,■ Ref. [7]; SVE data: ▲: Ref. [8]; – – : qualitative vapor compositions.

Preston and al. [9] used an equilibrium cell for measuring the solubility of solid neo-pentane in methane. Although experimental pressures were not reported in Ref. [9], the measured solubility of neo-pentane should correspond to SLVE condition seeing that the vapor phase originating within the equilibrium cell was recirculated with a peristaltic pump to accelerate attainment of the equilibrium between the phases and to provide stirring of the liquid phase. Considering the different volatility between methane and neo-pentane, this vapor phase can be roughly considered as pure methane, thus the experimental SLVE pressure can be approximated by the saturation pressure of pure methane at the experimental temperature.

To sum up, all the available literature values accounting for phase equilibria are represented by symbols in the pressure-temperature diagram of Figure 3 maintaining for VLE and S_2VE data the same symbolism of Figures 1-2, while the three S_2LVE values of Ref. [9] are pointed out by open circles.

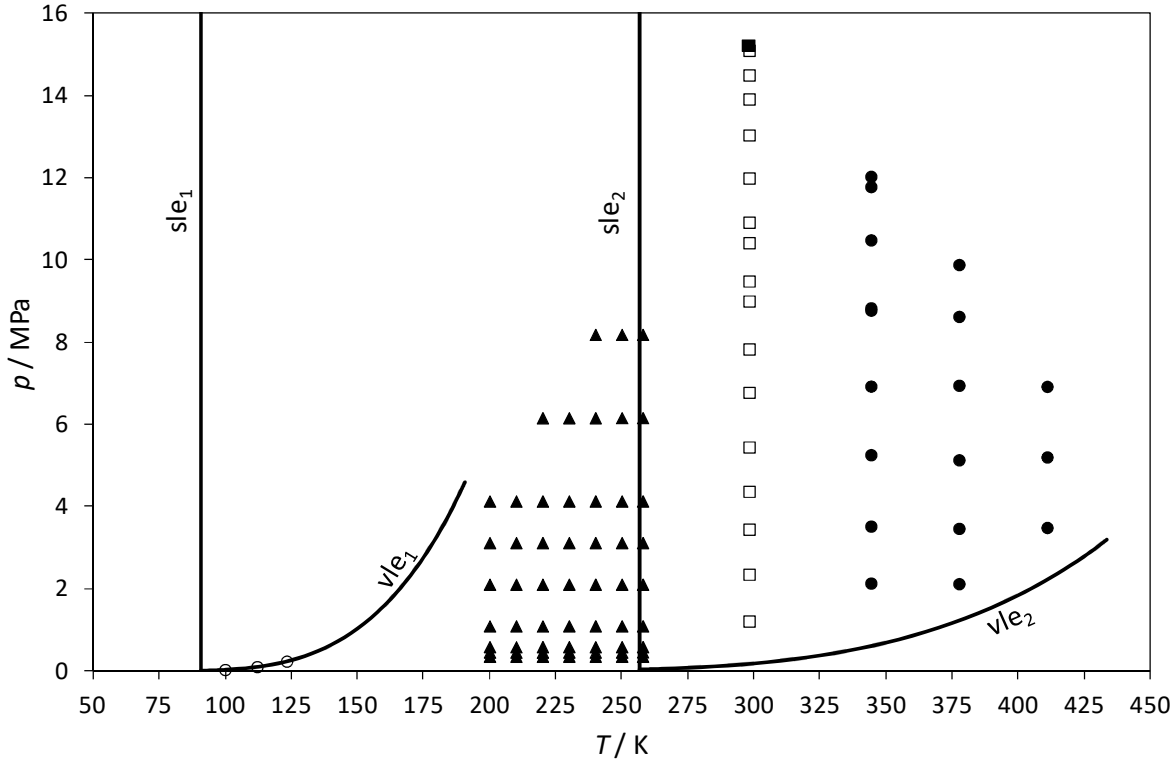

Figure 3. PT diagram for the CH_4+neo-C_5H_{12} system
Pure components properties: ▬ : saturation and melting lines.

VLE data: ● Ref. [6], □,■ Ref. [7]; SVE data: ▲ : Ref. [8]; S_2LVE data: ○ : Ref. [9].
Subscripts: 1 : related to methane; 2 : related to neo-pentane.

In Figure 3, saturation lines of methane and neo-pentane have been obtained by means of the GERG2008 Equation of State (EoS) [10] as implemented in REFPROP v.10 [11], whereas the vertical lines roughly represent the melting curves of methane and neo-pentane and are located at their triple-point temperatures (90.694 K and 256.6 K, see Table 1).

According to Figure 3 and in particular to the data given in [8], it can be stated that the vapor-liquid equilibrium behavior of the methane+neo-pentane system extends from the critical-point temperature of neo-pentane down to its triple-point temperature. For each pressure up to 8 MPa, the system is at solid-vapor equilibrium for temperatures lower than the solid-liquid temperature of neo-pentane down to the corresponding saturation temperature of methane.

The absence of low-temperature VLE data (VLE at temperatures lower than the triple-point temperature of neo-pentane) and the VLE behavior illustrated in Figure 1 (a critical-point pressure increasing for decreasing temperatures) suggest a fluid-phase diagram of type III (qualitatively shown in Figure 4) according to the van Konynenburg and Scott's classification, [12].

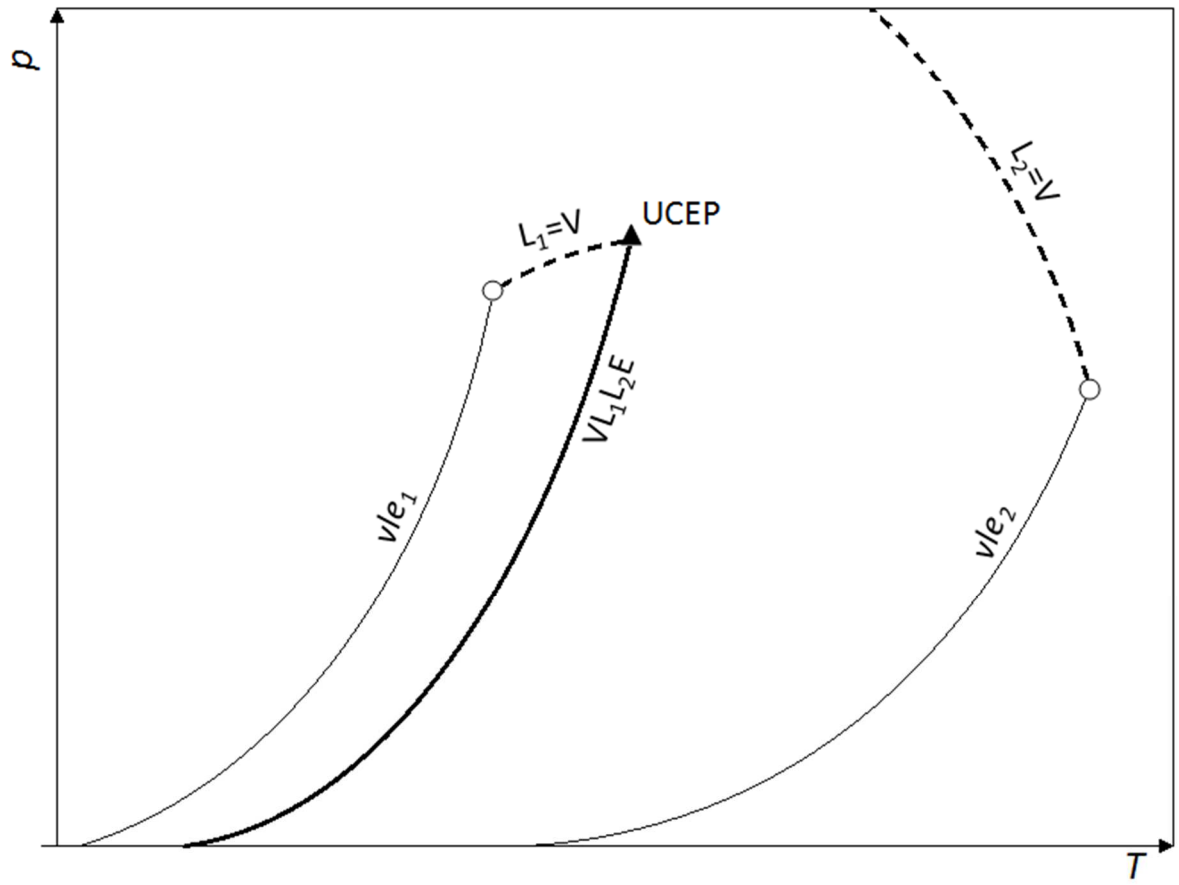

Figure 4. Qualitative PT fluid-phase diagram for the (1)CH_4+(2)neo-C_5H_{12} system inferred from available literature equilibrium values and according to the van Konynenburg and Scott's classification, [12].

Pure components properties: — : saturation line; ○ : critical point. Mixture properties: ▬ : 3-phase equilibrium locus; ▬ ▬ : critical locus; ▲ : upper critical end point. Subscripts: 1 : related to methane; 2 : related to neo-pentane.

As a consequence, a Vapor-Liquid-Liquid Equilibrium (VL_1L_2E) locus has been arbitrarily drawn in Figure 4 between the saturation curves of methane and neo-pentane. This VL_1L_2E curve represents the equilibrium between a vapor phase, a methane-rich liquid phase (L_1) and a neo-pentane-rich liquid phase (L_2), and extends from an Upper Critical End Point (UCEP) down to low pressures and temperatures. A first critical curve representing the coexistence of a vapor phase and the methane-rich liquid phase (L_1=V) exits the critical point of methane and ends at this UCEP. A second critical line representing the coexistence of a vapor phase and the neo-pentane-rich liquid phase (L_2=V) exits the critical point of neo-pentane and develops in the high pressure region.

Nevertheless, the VL_1L_2E locus becomes metastable when taking into account the phase equilibria involving solid phases. Indeed, (i) the high SVE pressures given in Ref. [8] at temperatures close to the triple-point temperature of neo-pentane and (ii) a miscibility gap in the solid phase (solid phases partially miscible or totally immiscible) suggest a global phase diagram of type A (qualitatively shown in Figure 5 down to 70 K) according to the Kohn and Luks' classification, [13].

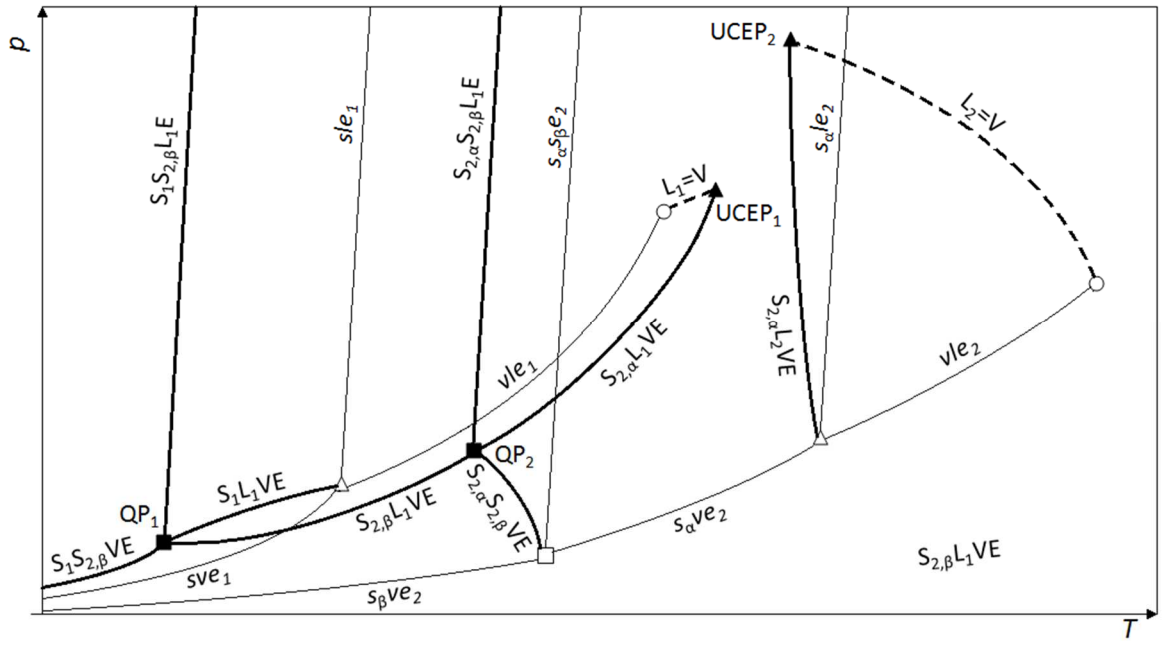

Figure 5. Qualitative PT global-phase diagram for the (1)CH_4+(2)neo-C_5H_{12} system down to 70 K inferred from available literature equilibrium values. The diagram is of type A according to the Kohn and Luks' classification, [13].

Pure components properties: — : saturation, melting, sublimation, and solid-solid transition lines; □ : solid-solid-vapor triple point of neo-pentane; Δ : solid-liquid-vapor triple point; ○ : critical point. Mixture properties: ▬ : 3-phase equilibrium locus; ▬ ▬ : critical locus; ▲ : upper critical end point; ■ : quadruple point. Subscripts: 1 : related to methane; 2 : related to neo-pentane; α,β: crystal structures of solid neo-pentane.

As a consequence, the methane+neo-pentane system is characterized by equilibria involving solid methane (S_1) and two crystal structures of solid neo-pentane ($S_{2,\alpha}$ and $S_{2,\beta}$) which result in the following 4 singular points:

- The “warmer” UCEP ($UCEP_2$), namely the ending point of both the L_2=V critical locus and the $Solid_{2,\alpha}$-$Liquid_2$-Vapor Equilibrium ($S_{2,\alpha}L_2VE$) locus;
- The “colder” UCEP ($UCEP_1$) namely the ending point of both the L_1=V critical locus and the $Solid_{2,\alpha}$-$Liquid_1$-Vapor Equilibrium ($S_{2,\alpha}L_1VE$) locus;
- The “warmer” Quadruple Point (QP_2), namely the meeting point of the $S_{2,\alpha}L_1VE$, the $Solid_{2,\alpha}$-$Solid_{2,\beta}$-Vapor Equilibrium ($S_{2,\alpha}S_{2,\beta}VE$), the $Solid_{2,\alpha}$-$Solid_{2,\beta}$-$Liquid_1$ Equilibrium ($S_{2,\alpha}S_{2,\beta}L_1E$), and the $Solid_{2,\beta}$-$Liquid_1$-Vapor Equilibrium ($S_{2,\beta}L_1VE$) loci;
- The “colder” Quadruple Point (QP_1), namely the meeting point of the $S_{2,\beta}L_1VE$, the $Solid_1$-$Solid_{2,\beta}$-Vapor Equilibrium ($S_1S_{2,\beta}VE$), the $Solid_1$-$Solid_{2,\beta}$-$Liquid_1$ Equilibrium ($S_1S_{2,\beta}L_1E$), and the $Solid_1$-$Liquid_1$-Vapor Equilibrium (S_1L_1VE) loci.

3. Global phase equilibrium behavior from predictive thermodynamic models

The phase equilibrium behavior of the methane+neo-pentane system involving solid phases has been predicted by using a thermodynamic model consisting of a predictive Equation of State (EoS) for calculating the fluid-phase properties, and a solid-phase model for calculating the fugacity of neo-pentane and methane in their solid states. In this work, it has been assumed that the system is characterized by pure solid phases (solid methane and solid neo-pentane are then totally immiscible): solid methane (S_1 phase), solid neo-pentane with structure α ($S_{2,\alpha}$ phase), and solid neo-pentane with structure β ($S_{2,\beta}$ phase).

Two predictive fluid-phase models, the Predictive Peng-Robinson (PPR78) EoS, [14], and the Predictive Soave Redlich-Kwong (PSRK) EoS, [15], have been coupled one by one with the so-called Classical Approach (CA) for the solid phase, [16]. For the properties of the fluid phases, calculations have been performed by means of the two predictive models as implemented in Simulis Thermodynamics Software, [17].

At the system temperature (T) and pressure (p), the necessary prerequisite for the thermodynamic equilibrium is the isofugacity condition between the partial molar fugacities $\hat{f}$ in all the (γ, δ, ε, …) equilibrium phases for each i^{th}-component in the mixture:

$$\hat{f}_i^{\gamma}\left(T, p, \bar{x}_{\gamma}\right) = \hat{f}_i^{\delta}(T, p, \bar{x}_{\delta}) = \hat{f}_i^{\varepsilon}(T, p, \bar{x}_{\varepsilon}) = \cdots \quad (1)$$

where $\bar{x}_{\gamma}$, $\bar{x}_{\delta}$, and $\bar{x}_{\varepsilon}$ are the vectors of compositions in the γ, δ, and ε phase, respectively.

The partial molar fugacities of the generic i^{th}-component in the mixture (methane and neo-pentane) in the vapor and liquid phases have been calculated by means of the PPR78 and PSRK EoSs and can be expressed in terms of partial molar fugacity coefficients:

$$\hat{f}_i^{V}(T, p, \bar{y}) = y_i \hat{\varphi}_i^{V} p \quad (2)$$

$$\hat{f}_i^{L}(T, p, \bar{x}) = x_i \hat{\varphi}_i^{L} p \quad (3)$$

where $\bar{y}$ is the vector of composition of the vapor phase, $\bar{x}$ is the vector of composition of the liquid phase, $\hat{\varphi}_i^V$ and $\hat{\varphi}_i^L$ are the partial molar fugacity coefficients of component *i* in the vapor and liquid phase, respectively.

Neglecting pressure effects and the term involving the isobaric heat capacity change upon melting, the CA applied for the S_1, $S_{2,\alpha}$, $S_{2,\beta}$ phases yields:

$$f_1^S(T,p) = f_1^L(T,p)exp\left\{\frac{1}{RT}\left[\Delta H_1^{SLE}\left(\frac{T}{T_{t,1}}-1\right)\right]\right\} \quad (4)$$

$$f_{2,\alpha}^S(T,p) = f_2^L(T,p)exp\left\{\frac{1}{RT}\left[\Delta H_2^{SLE}\left(\frac{T}{T_{t,2}}-1\right)\right]\right\} \quad (5)$$

$$f_{2,\beta}^S(T,p) = f_2^L(T,p)exp\left\{\frac{1}{RT}\left[\Delta H_2^{SLE}\left(\frac{T}{T_{t,2}}-1\right)+\Delta H_2^{SSE}\left(\frac{T}{T_{2,ss}}-1\right)\right]\right\} \quad (6)$$

where *R* is the gas constant, *T* is the system temperature, $T_{t,i}$ and ΔH_i^{SLE} are the triple-point temperature and latent heat of melting of component *i* (1 = methane, 2 = neo-pentane), respectively, $T_{2,ss}$ and ΔH_2^{SSE} are the solid-solid transition temperature of neo-pentane and related latent heat, respectively. In Eqs. (4)-(6), f_i^S and f_i^L are the fugacity of the pure component *i* in the solid and liquid phase, respectively, at the system pressure and temperature (the effect of the pressure on the solid fugacity is given by the one on the liquid fugacity since no additional pressure-dependent terms are present in the right-hand side of the previous three equations).

It should be kept in mind that applying Eqs. (4)-(6) and considering pure solid phases means that, for instance at a solid-fluid equilibrium, the isofugacity condition applies only for the component composing the pure solid phase.

The global phase diagram of the binary mixture treated in this work has been obtained by combining Eqs. (2)-(6) to predict first the complete boundary equilibrium conditions of the pure components. Secondly, the prediction has involved the phase equilibrium behavior of the mixture: critical locus (L=V), all the 3-phase equilibrium loci (Solid-Liquid-Vapor, Solid-

Solid-Liquid, Liquid-Liquid-Vapor, and Solid-Solid-Vapor equilibria) and singular points (Upper Critical End Points and Quadruple Points).

In the following the main outcomes of the modeling work are resumed (please refer to the Supplementary Material S1 for details concerning the procedure used for the calculation of the different kind of equilibrium):

- The global phase diagrams of pure methane and neo-pentane down to 70 K and for pressures from 1 mPa (10^{-3} Pa) up to 10 MPa as calculated by coupling the PSRK EoS and the CA are portrayed in Figure 6. Similar results have been obtained when replacing the PSRK EoS with the PPR78 EoS.

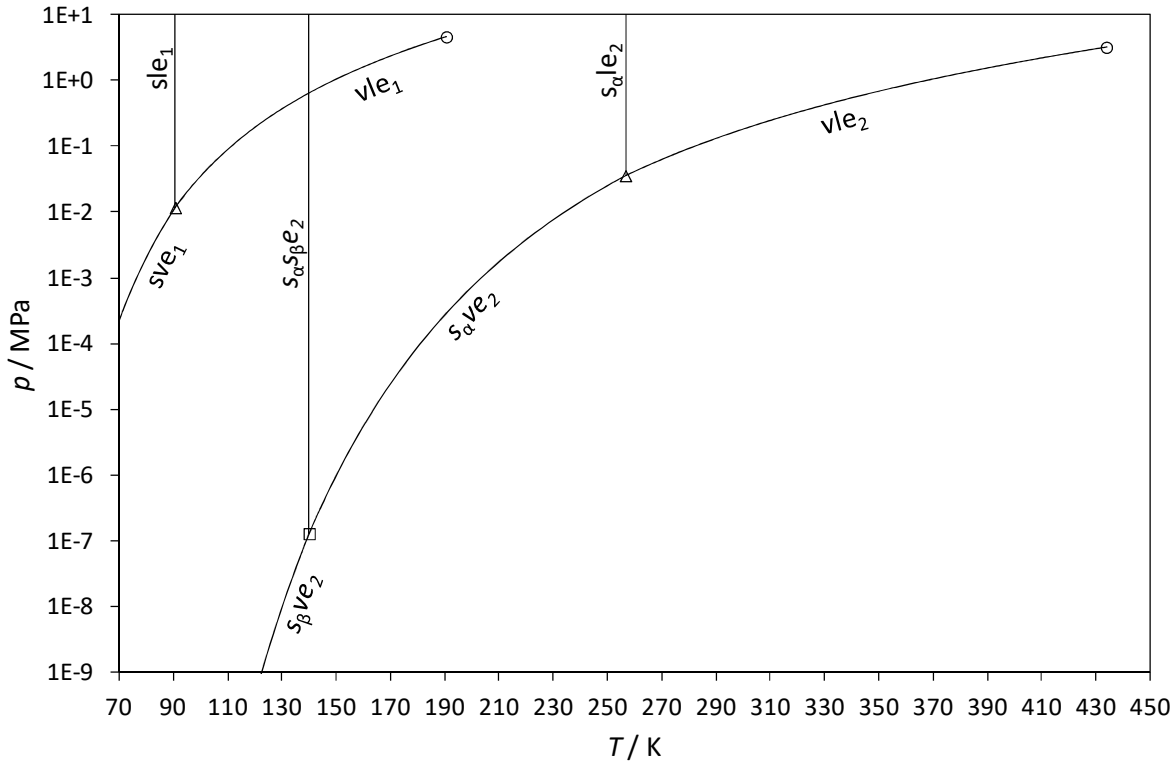

Figure 6. Calculated global phase diagrams of methane and neo-pentane down to 70 K. — : saturation, melting, sublimation, and solid-solid transition lines; Δ : solid-liquid-vapor triple point; □ : solid-solid-vapor triple point of neo-pentane; ○ : critical point. Subscripts: 1 : related to methane; 2 : related to neo-pentane; α,β: crystal structures of solid neo-pentane. Solid-phase model: Classical Approach; Fluid-phase model: PSRK EoS.

- The modeling of the behavior of the methane+neo-pentane system at critical conditions with both the PPR78 and PSRK EoSs has provided a continuous critical line that joins the critical points of the two pure components as illustrated in Figure 7.

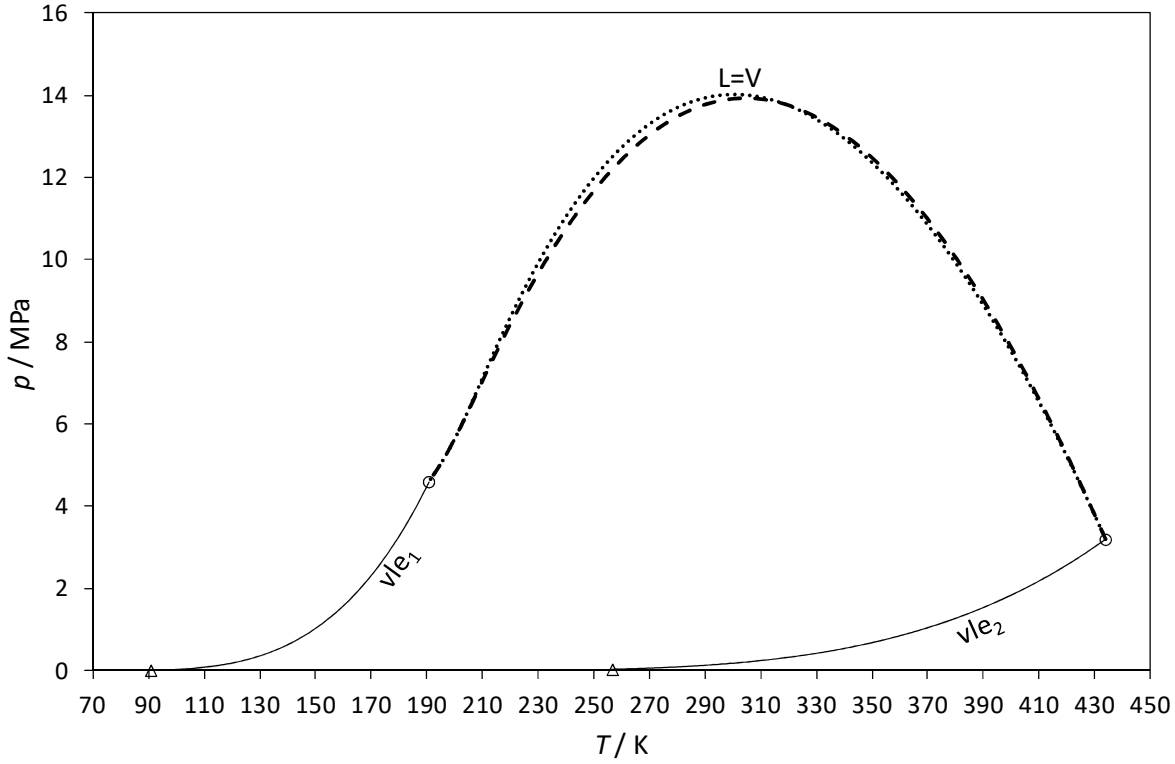

Figure 7. Calculated critical locus of the (1)CH_4+(2)neo-C_5H_{12} system.
Pure component properties: — : saturation line (PSRK EoS); Δ : solid-liquid-vapor triple point (PSRK EoS); ○ : critical point (PSRK EoS).
Critical line of the mixture: ▬ ▬ (PPR78 EoS), ••• (PSRK EoS).
Subscripts: 1 : related to methane; 2 : related to neo-pentane.

In addition to that, no further critical conditions have been encountered for this system from the modeling point of view, and this implies that the mixture does not present a demixing in the liquid phase (then nor liquid-liquid nor liquid-liquid-vapor equilibria) at least in the investigated temperature-pressure range. As a consequence, the modeling of singular points of the system has not involved the calculation of Upper Critical End Points and has only focused on the determination of the Quadruple Points. The

calculated phase equilibrium properties of the methane+neo-pentane system at the two quadruple points are gathered in Table 3.

Table 3. Calculated quadruple points of the methane+neo-pentane system.
$z_{1,1}$: molar composition of methane in the solid$_1$ phase (pure methane); $z_{1,2\alpha}$: molar composition of methane in the solid$_{2,\alpha}$ phase (pure neo-pentane with crystal α-structure); $z_{1,2\beta}$: molar composition of methane in the solid$_{2,\beta}$ phase (pure neo-pentane with crystal β-structure); x_1 : molar composition of methane in the liquid phase; y_2 : molar composition of neo-pentane in the vapor phase.

Fluid-phase model	QP	T K	p MPa	$z_{1,1}$ mol/mol	$z_{1,2\alpha}$ mol/mol	$z_{1,2\beta}$ mol/mol	x_1 mol/mol	y_2 mol/mol
PPR78 EoS	$S_{2,\alpha}S_{2,\beta}$LVE	140.0	0.3588	-	0	0	0.6541	1.63×10^{-3}
	$S_1S_{2,\beta}$LVE	76.35	1.02×10^{-3}	1	-	0	0.8958	4.55×10^{-15}
PSRK EoS	$S_{2,\alpha}S_{2,\beta}$LVE	140.0	0.5669	-	0	0	0.8489	4.65×10^{-7}
	$S_1S_{2,\beta}$LVE	90.48	1.13×10^{-2}	1	-	0	0.9970	2.84×10^{-14}

According to the results within Table 3, it is possible to state that the vapor phases at $S_{2,\alpha}S_{2,\beta}$LVE and $S_1S_{2,\beta}$LVE are mainly composed by methane. The molar composition of methane in the liquid phases at the two quadruple points predicted by coupling the PPR78 EoS with the CA are lower than the corresponding values obtained when the PSRK EoS is used (about 0.65 and 0.90 against about 0.85 and 0.997). With respect to the QP occurring in response to the solid-solid transition of neo-pentane ($S_{2,\alpha}S_{2,\beta}$LVE), the use of the PSRK EoS results in a higher equilibrium pressure (about 0.57 bar) than using the PPR78 EoS (about 0.36 bar). Similarly, the predicted $S_1S_{2,\beta}$LVE temperature is higher when the PSRK EoS is used (90.48 K against 76.35 K calculated when the fluid-phase behavior is predicted with the PPR78 EoS).

- The modeling of the 3-phase equilibria of the methane+neo-pentane system is portrayed in Figures 8-10.

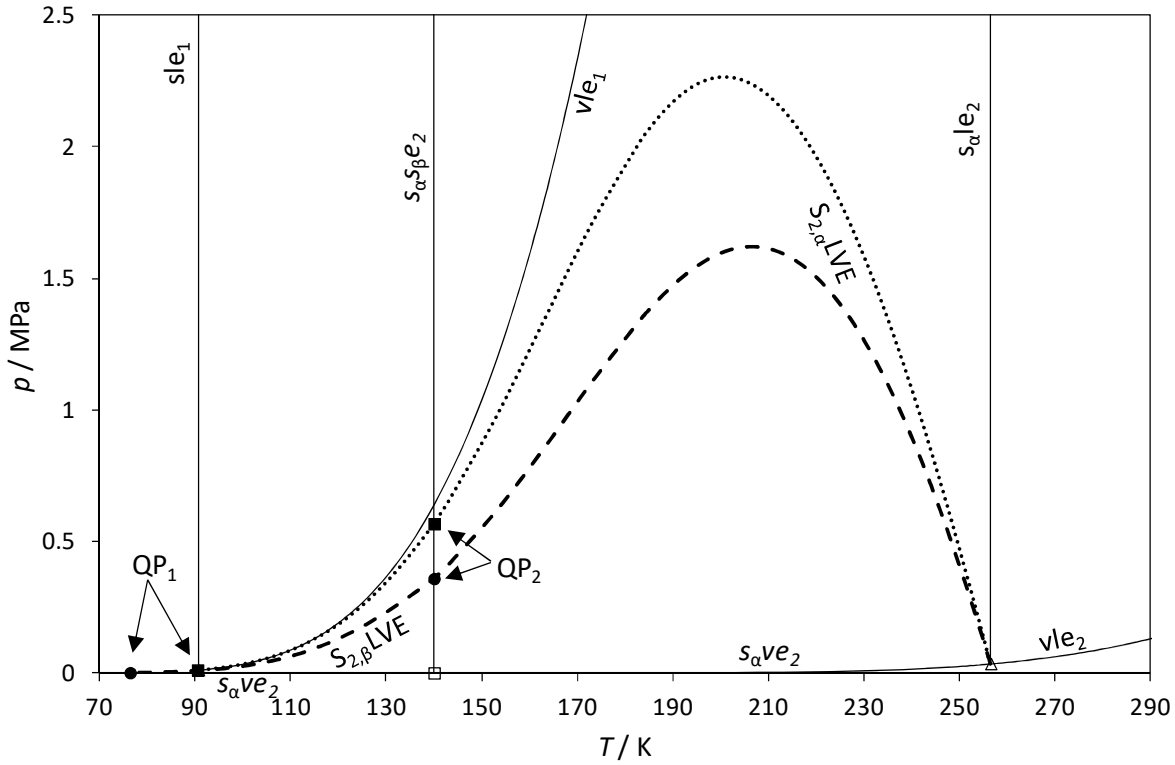

Figure 8. Calculated S_2LVE and QPs of the (1)CH_4+(2)neo-C_5H_{12} system.
Pure component properties: — : saturation, melting, sublimation, and solid-solid transition lines (PSRK EoS); □ : solid-solid-vapor triple point of neo-pentane; Δ : solid-liquid-vapor triple point.
Mixture properties: S_2LVE line: ▬ ▬ (PPR78 EoS), ••• (PSRK EoS); QPs: ● (PPR78 EoS), ■ (PSRK EoS). Subscripts: 1 : related to methane; 2 : related to neo-pentane. Solid-phase model: Classical Approach.

As illustrated in Figure 8, the $S_{2\alpha,\beta}$LVE pressures predicted by coupling the PSRK EoS and the CA are higher than the values obtained when the PPR78 EoS is used (in agreement with the pressures of the "warmer" quadruple points given in Table 3). Figure 9 illustrates the phase equilibrium behavior calculated by coupling the PPR78 EoS and the CA for temperatures between 110 K and 290 K. The $S_{2,\alpha}S_{2,\beta}$VE runs from the solid$_\alpha$-solid$_\beta$-vapor triple-point temperature of neo-pentane up to the "warmer" quadruple point (QP_2), whereas the $S_{2,\alpha}S_{2,\beta}$LE branch exits this last singular point and develops in the high pressure region. In addition to that, the solid-solid equilibrium ($s_\alpha s_\beta e$) line is totally overlapped by the $S_{2,\alpha}S_{2,\beta}$LE and $S_{2,\alpha}S_{2,\beta}$VE branches in Figure 9.

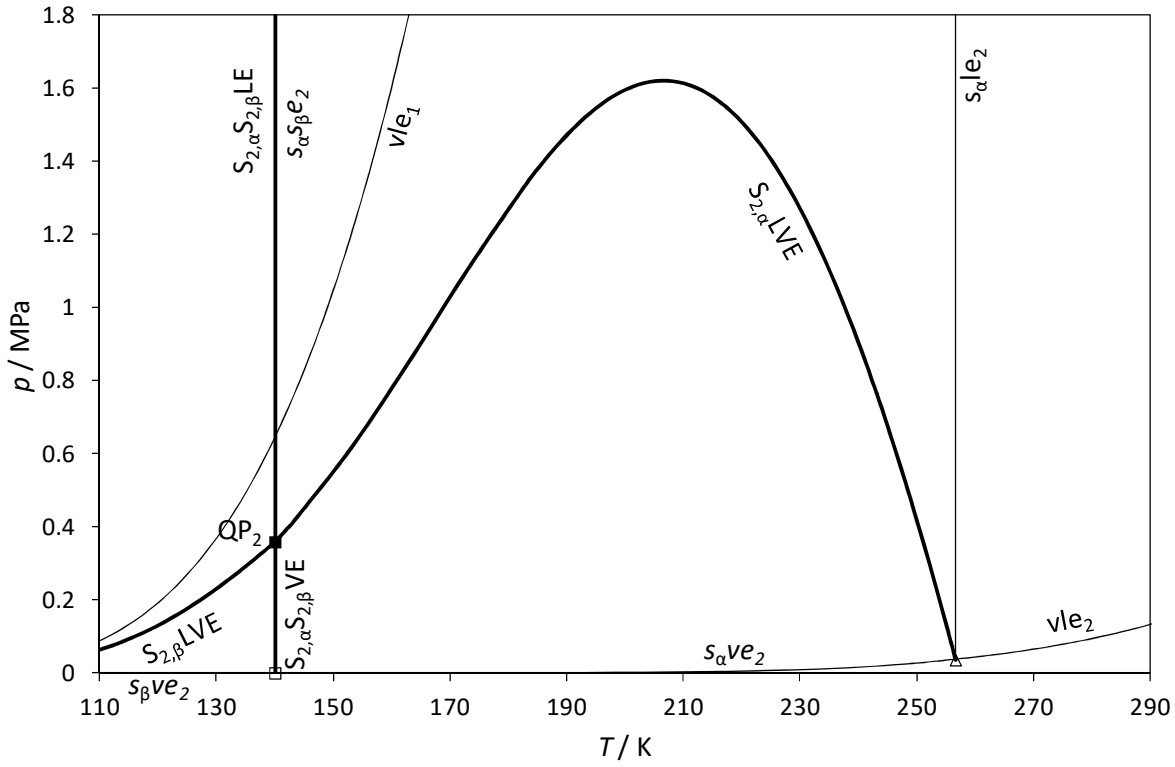

Figure 9. Calculated $S_{2\alpha}S_{2\beta}$VE, $S_{2\alpha}S_{2\beta}$LE, S_2LVE, and QP_2 of the (1)CH_4+(2)neo-C_5H_{12} system.

Pure component properties: — : saturation, melting, sublimation, and solid-solid transition lines; Δ : solid-liquid-vapor triple point of neo-pentane; □ : solid-solid-vapor triple point of neo-pentane.

Mixture properties: ▬ : 3-phase equilibrium lines; ■ : QP_2 ($S_{2\alpha}S_{2\beta}$LVE).

Subscripts: 1 : related to methane; 2 : related to neo-pentane.

Solid-phase model: Classical Approach; Fluid-phase model: PPR78 EoS.

The remaining low-temperature 3-phase equilibrium loci (the S_1LVE, $S_1S_{2\beta}$VE, and $S_1S_{2\beta}$LE branches) calculated when the PPR78 EoS is coupled with the CA are illustrated in Figure 10. For the reader convenience, it should be noticed that in Figures 8-10 the sublimation line of methane and neo-pentane (sve_1, $s_\alpha ve_2$, and $s_\beta ve_2$ lines) develops in the very-low pressure region and are then often not visible.

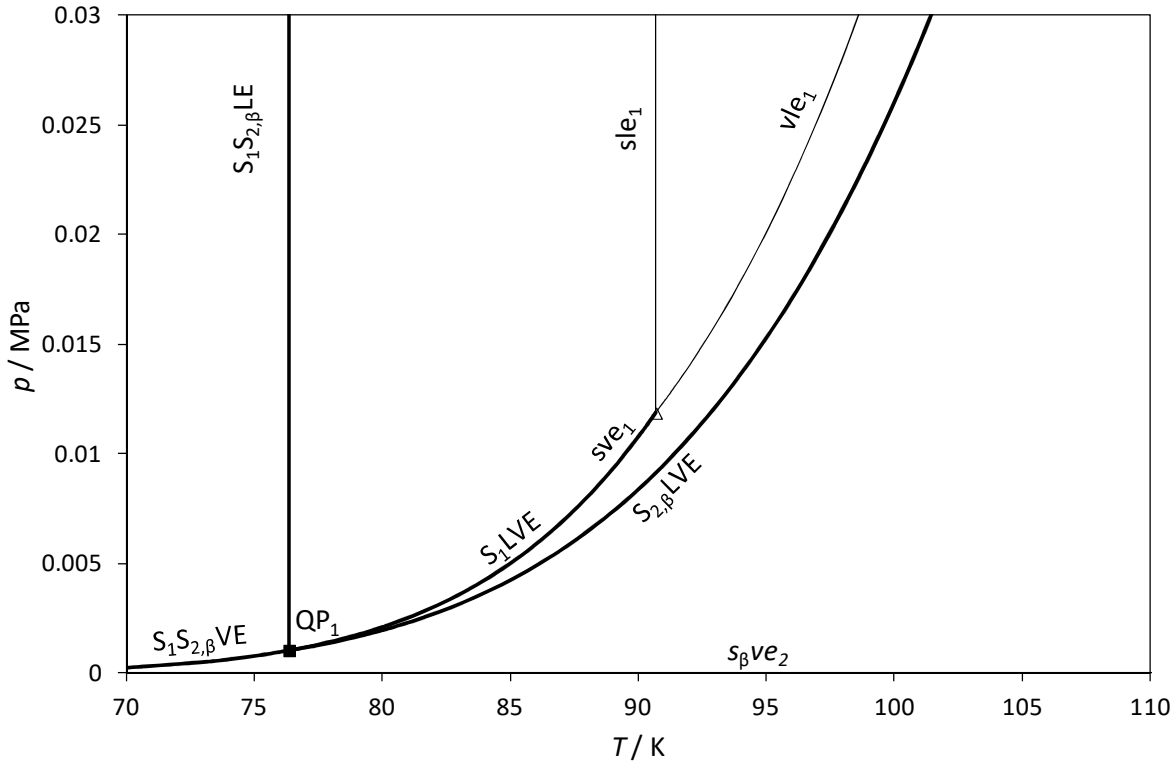

Figure 10. Calculated $S_1S_{2\beta}VE$, $S_1S_{2\beta}LE$, S_1LVE, $S_{2\beta}LVE$, and QP_1 of the (1)CH_4+(2)neo-C_5H_{12} system.

Pure component properties: — : saturation, melting, and sublimation lines; Δ : solid-liquid-vapor triple point. Mixture properties: ▬ : 3-phase equilibrium lines; ■ : QP_1 ($S_1S_{2\beta}LVE$).
Subscripts: 1 : related to methane; 2 : related to neo-pentane.
Solid-phase model: Classical Approach; Fluid-phase model: PPR78 EoS.

The global phase equilibrium behavior of the methane+neo-pentane system as calculated by coupling the PPR78 EoS and the CA is portrayed in Figure 11, whereas a zoom in the low-pressure – low-temperature region emphasizing the two quadruple points is shown in Figure 12.

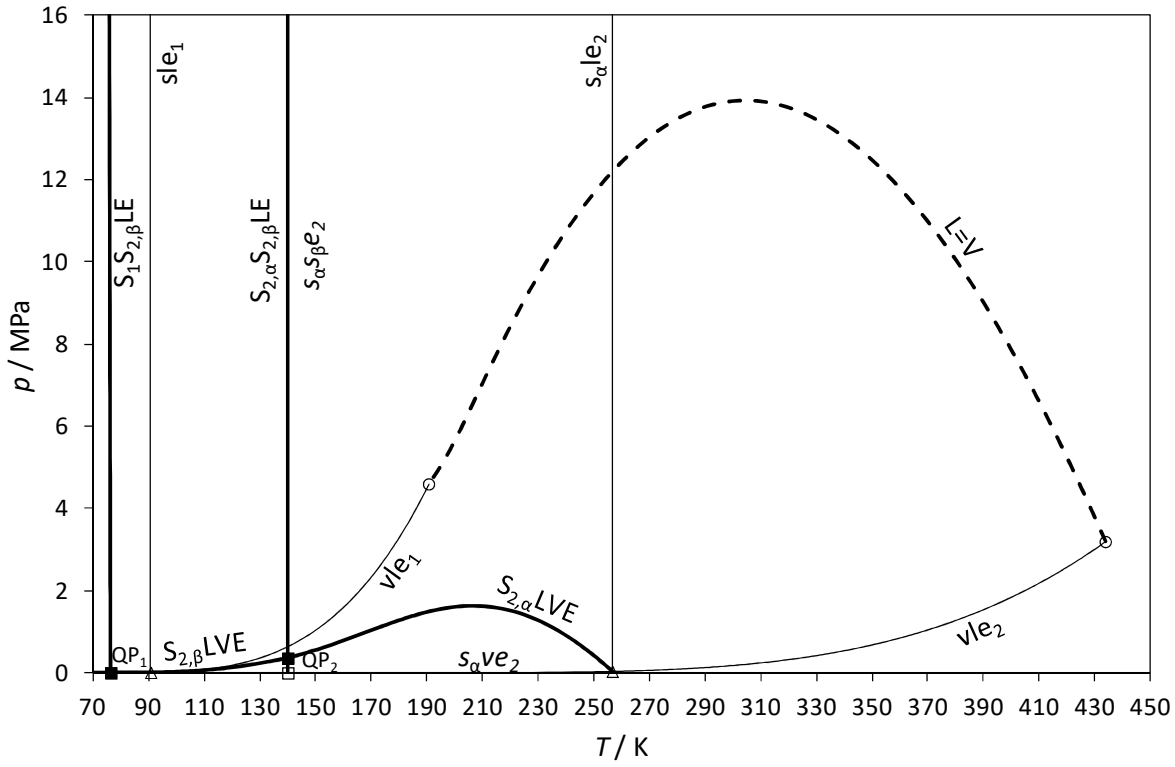

Figure 11. Calculated global phase diagram of the (1)CH_4+(2)neo-C_5H_{12} system down to 70 K.

Pure component properties: — : saturation, melting, sublimation, and solid-solid transition lines; Δ : solid-liquid-vapor triple point; □ : solid-solid-vapor triple point of neo-pentane. Mixture properties: ▬ : 3-phase equilibrium lines; ■ : QP_1 ($S_1S_{2\beta}LVE$) and QP_2 ($S_{2\alpha}S_{2\beta}LVE$); ▬ ▬ : critical line. Subscripts: 1 : related to methane; 2 : related to neo-pentane. Solid-phase model: Classical Approach; Fluid-phase model: PPR78 EoS.

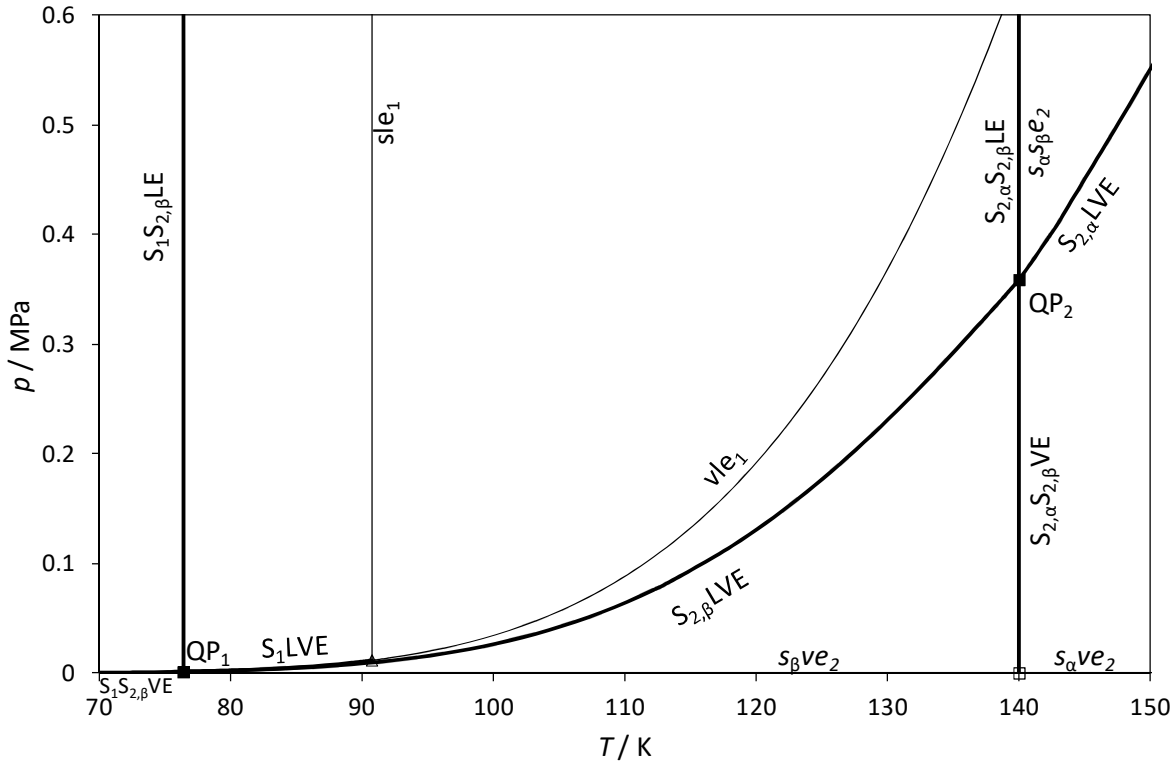

Figure 12. Calculated lowP-lowT global phase diagram of the (1)CH_4+(2)neo-C_5H_{12} system down to 70 K.

Pure component properties: — : saturation, melting, sublimation, and solid-solid transition lines; Δ : solid-liquid-vapor triple point of methane; □ : solid-solid-vapor triple point of neo-pentane. Mixture properties: ▬ : 3-phase equilibrium lines; ■ : QP_1 ($S_1S_{2\beta}LVE$) and QP_2 ($S_{2\alpha}S_{2\beta}LVE$).

Subscripts: 1 : related to methane; 2 : related to neo-pentane.

Solid-phase model: Classical Approach; Fluid-phase model: PPR78 EoS.

To sum up, the fluid-phase equilibrium behavior of the mixture as calculated by two predictive models (PPR78 EoS and PSRK EoSs) is of type I according to the van Konynenburg and Scott's classification, [12]. The global phase equilibrium behavior of the mixture down to 70 K as calculated by coupling the PPR78 EoS or the PSRK EoS for the fluid phase with a solid-phase fugacity model (CA) is of type D according to the Kohn and Luks' classification, [13]. To end this section, the global phase equilibrium behavior of the mixture is qualitatively illustrated in Figure 13.

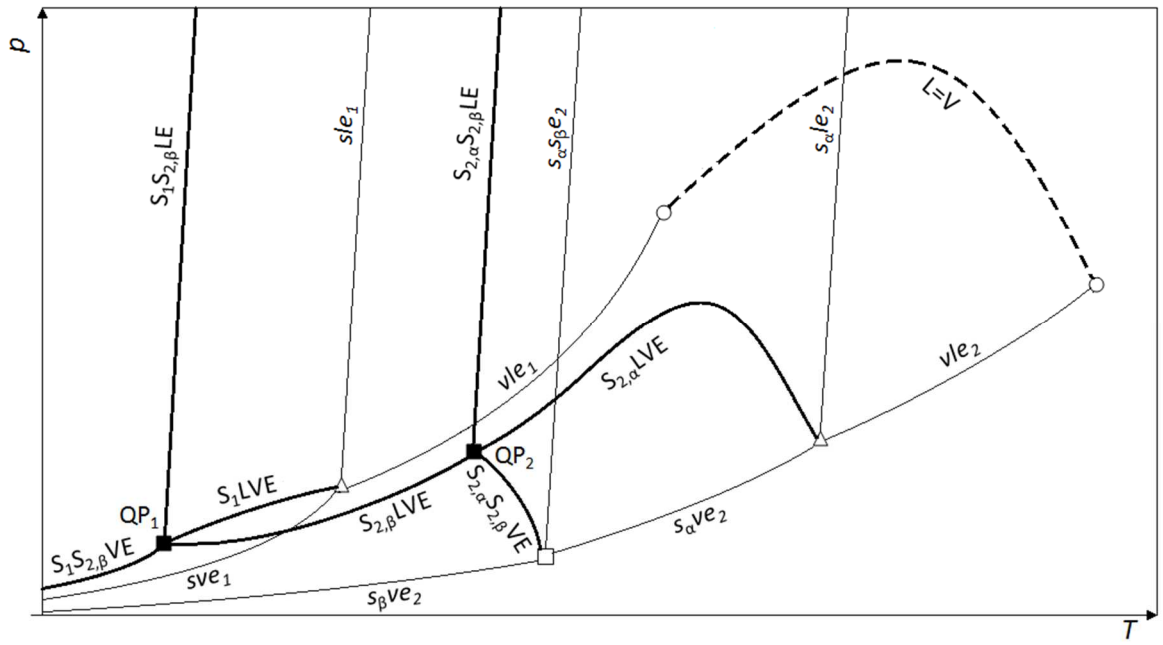

Figure 13. Qualitative PT global-phase diagram for the (1)CH_4+(2)neo-C_5H_{12} system down to 70 K according to modeling results. The diagram is of type D according to the Kohn and Luks' classification, [13].

Pure components properties: — : saturation, melting, sublimation, and solid-solid transition lines; □ : solid-solid-vapor triple point of neo-pentane; Δ : solid-liquid-vapor triple point; ○ : critical point. Mixture properties: ▬ : 3-phase equilibrium locus; ▬ ▬ : critical locus; ■ : quadruple point. Subscripts: 1 : related to methane; 2 : related to neo-pentane; α,β: crystal structures of solid neo-pentane.

4. Low-temperature VLE measurements

One notices at once that two partially different global phase diagrams for the methane+neo-pentane system are depicted in Figures 5 and 13.

In the temperature range from the critical-point temperature of methane up to the triple-point temperature of neo-pentane, the global phase diagram inferred from literature equilibrium values available in the open literature presents two different critical loci (phase diagram of type III according to the van Konynenburg and Scott's classification, [12]) ending at their corresponding UCEPs. As detailed at the end of section 2, these UCEPs limit also two $S_{2\alpha}LVE$ branches; the $S_{2\alpha}L_2VE$ branch ends at the $UCEP_2$ the $S_{2\alpha}L_1VE$ branch ends at the $UCEP_1$, where the L_2 and L_1 phases are a neo-pentane-rich and a methane-rich liquid phase, respectively.

To the contrary, the modeling of the phase equilibrium behavior by means of two common predictive fluid-phase models and a solid-fugacity model revealed a continuous critical line (phase diagram of type I according to the van Konynenburg and Scott's classification, [12]), and a continuous $S_{2\alpha}LVE$ branch. Along this 3-phase equilibrium locus, the composition of methane in the liquid phase x_1 increases from the value at the triple-point of neo-pentane (x_1 = 0) up to the value at the QP_2 (x_1 = 0.6541 or 0.8489 according to the fluid-phase model, see Table 3) without encountering any UCEP.

To sum up, literature values for the methane+neo-pentane system (basically the SVE data given in [8]) are a proof of the absence of equilibria other than the SVE at least up to 80 bar and in the temperature range from the $UCEP_1$ up to the $UCEP_2$, since the liquid phases end either at the temperature of the $UCEP_1$ (liquid phase richer in methane) or at the one of $UCEP_2$ (liquid phase richer in neo-pentane).

In order to gain some insights into the phase equilibrium behavior of the system treated in this work and to verify if the disagreement between the global phase diagrams illustrated in Figures 5 and 13 could be related to either a lack of further experimental values in the literature or to a

poor predictive capacity of the thermodynamic models, an experimental investigation has been carried out for temperatures ranging from 344 K down to 213 K.

4.1 Materials and apparatus

The details concerning the chemicals (suppliers, CAS numbers and stated purities) are gathered in Table 4.

Table 4. Purities and suppliers of the chemicals used in this work.

Chemical name	CAS number	Purity "*P*" (mol/mol)	Source
methane	74-82-8	0.99995	MESSER
neo-pentane	463-82-1	0.99	AIR LIQUIDE

The equipment used for the evaluation of the phase equilibrium behavior is based on a ″static-analytic″ method with liquid and vapor phase samplings. The equipment is similar to that presented in Ref. [18] and its flow diagram is presented in Figure 14.

The sapphire equilibrium cell is totally submerged into a thermo-regulated liquid bath maintained at the setpoint temperature imposed via a temperature regulator. The cell is equipped with two platinum resistance thermometer Pt-100 probes (located in the top and bottom flange, respectively) and with two pressure transducers (DRUCK type PTX611, range: 0-5 MPa, type PTX611, range: 0-20 MPa). Temperature probes have been calibrated against a 25Ω reference platinum probe (Pt25, Hart Scientific, reference uncertainty u_{REF} = 8 mK). The reference platinum resistance thermometer was calibrated by the Laboratoire National d'Essais de Paris following the ITS90 (1990 International Temperature Scale) protocol. The maximum absolute deviation (b_T) given by the calibration of the Pt100 probes is 16 mK for the bottom Pt-100 probe and 20 mK for the top Pt-100 probe.

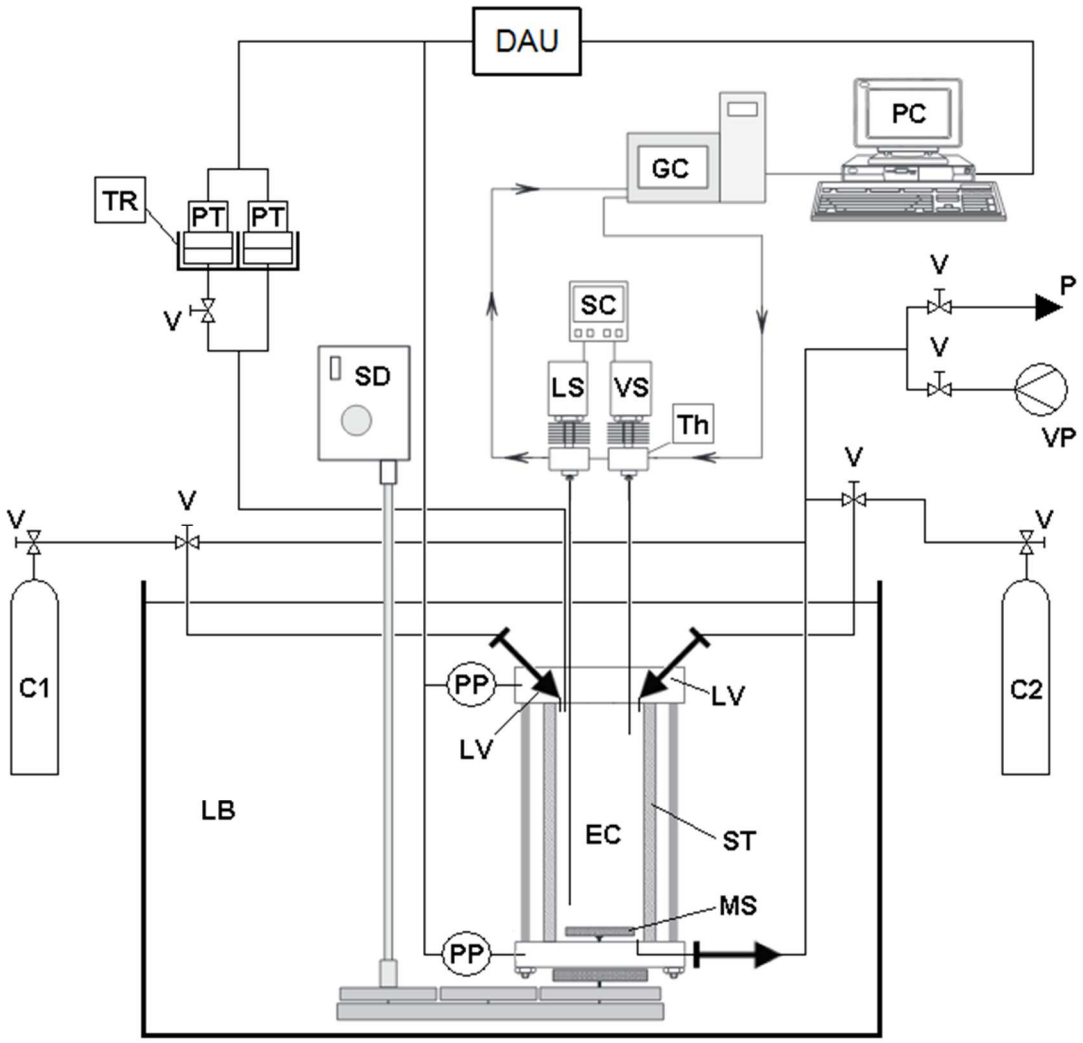

Figure 14. Flow diagram of the static-analytic apparatus

C1 : methane; C2 : neo-pentane; DAU : data acquisition unit; EC : equilibrium cell; GC : gas chromatograph; LB : liquid bath; LS : liquid ROLSI® sampler; LV: loading valve; MS : magnetic stirrer; P : Purge; PC : personal computer; PP : platinum resistance thermometer probe; PT : pressure transducer; SC : sample controller; SD : stirring device; ST : sapphire tube TR : temperature regulator; Th : thermocouple; V : valve; VP : vacuum pump; VS : vapor ROLSI® sampler.

Pressure transducers are maintained at constant temperature by means of a heating cartridge and have been calibrated against a PACE 5000 modular pressure controller (Desgranges&Huot, reference uncertainty u_{REF} = 0.09 kPa). The maximum absolute deviations (b_P) given by the calibration of the pressure transducers are 0.4 kPa for the “0-5 MPa” transducer and 1.8 kPa for the “0-20 MPa” transducer.

These four sensors (Pt100 probes and DRUCK transducers) are connected to a data acquisition unit (HP34970A) for temperature and pressure readings. The use of two Pt100 probes allows the quantification of any temperature gradient along the vertical axis of the equilibrium cell and the experimental temperature is the average of the two temperature measurements (obtained after correction of the temperature readings of the two Pt100 probes by means of the corresponding calibration polynomials). The experimental pressure corresponds to the reading of the pressure transducer chosen according to the working conditions (pressure generated by the system) after correction via the corresponding calibration polynomial.

Samples of the equilibrium phases within the cell are withdrawn thanks to two ROLSI® samplers, [19], vaporized in the heated chamber of the ROLSI® samplers and mixed with the carrier gas (helium) into the transfer line, then directly injected into the analytical circuit toward the head of the column (Porapak R 80/100 mesh; 1/8" Silcosteel tube, 2m length, 2mm internal diameter, Restek) located in the oven of the gas chromatograph (PERICHROM Model PR2100), and finally analyzed by a Thermal Conductivity Detector (TCD) connected to an acquisition system (WINILAB III).

The response of the TCD is calibrated by injecting known amounts of pure methane and pure neo-pentane into the Gas Chromatograph (GC) using an automatic syringe (Evol from SGE). For each component, the obtained polynomial relates the known numbers of moles injected in the GC's column to the surfaces of the GC's peaks; such polynomials are then used backward during the experimental campaign to determine the number of moles of neo-pentane and methane present in the liquid or vapor samples starting from the GC's peaks for determining their molar composition. The maximum absolute relative deviation (b_N) given by the calibration of the response of the TCD is estimated to be within 1.2% for methane and 0.8% for neo-pentane.

Keeping into account the purity of methane and neo-pentane given in Table 4, the chromatographic device used for VLE measurements has been used for determining the ratio between the surface of the GC's peak of each chemical of interest (methane or neo-pentane) and the sum of the surfaces of all the peaks obtained after GCA (surface of the chemical of interest plus all the surfaces of unknown components representing the stated impurity). The obtained surface ratio of methane obtained by sampling supercritical methane loaded in the equilibrium cell is higher than 99.9% (average of a total of 10 samples); the obtained surface ratio of (neo-pentane) obtained by sampling vapor and liquid neo-pentane loaded in the equilibrium cell is of about 99,7% (average of a total of 10 samples); these values agree with the purity stated by the suppliers.

In Figure 15, the vapor pressure of neo-pentane measured between 260 K and 350 K with the experimental apparatus is compared to the saturation line calculated from the reference equation of state of neo-pentane given in Ref. [1] as implemented in Ref. [11]; corresponding experimental values are gathered in Table 5. In Table 5, relative expandend combined uncertainty affecting experimental temperature and pressure is given in the 2^{nd} and 4^{th} column, respectively; the percentage relative deviations between measured values and values calculated from Ref. [1] are in the last two columns.

There is a good agreement between the experimental and calculated VLE conditions: at given pressure (temperature), the absolute value of the percentage relative deviation err_T (err_P) between calculated and experimental VLE temperatures (pressures) never exceeds 0.23% (1.78%). These deviations could be explained by the use of neo-pentane with 1% mol/mol of impurities, of 2^{nd} order calibration polynomials for the temperature probes covering a large temperature range (from 200 K up to 400 K), and of a 2^{nd} order calibration polynomial for the pressure transducer covering a large pressure range (0-5 MPa).

Readers can refer to the Supplementary Material S2 for the quantitative comparison between literature VLE data of neo-pentane, data within Table 5, and values calculated with the reference equation of state of neo-pentane given in Ref. [1].

Table 5. Experimental VLE of neo-pentane from 260 K up to 350 K.
$U^{REL}(M)$: relative expanded (k=2) combined uncertainty of property M, $U^{REL}(M) = 2 \times u(M) / M$; $err\_M = 100 \times (M^{CAL} - M^{EXP}) / M^{EXP}$.

T K	$U^{REL}(T)$ %	p kPa	$U^{REL}(p)$ %	err_T %	err_P %
353.71	0.01	733.04	0.61	-0.23	1.77
341.74	0.01	557.73	0.80	-0.22	1.78
332.93	0.01	450.67	0.99	-0.20	1.66
322.88	0.01	347.56	1.28	-0.19	1.62
312.92	0.01	264.99	1.68	-0.13	1.18
302.96	0.01	197.26	2.25	-0.11	1.09
293.00	0.01	144.29	3.08	-0.05	0.48
283.02	0.01	102.41	4.34	-0.03	0.25
273.01	0.01	70.88	6.27	0.05	-0.50
263.05	0.01	47.55	9.35	0.12	-1.23

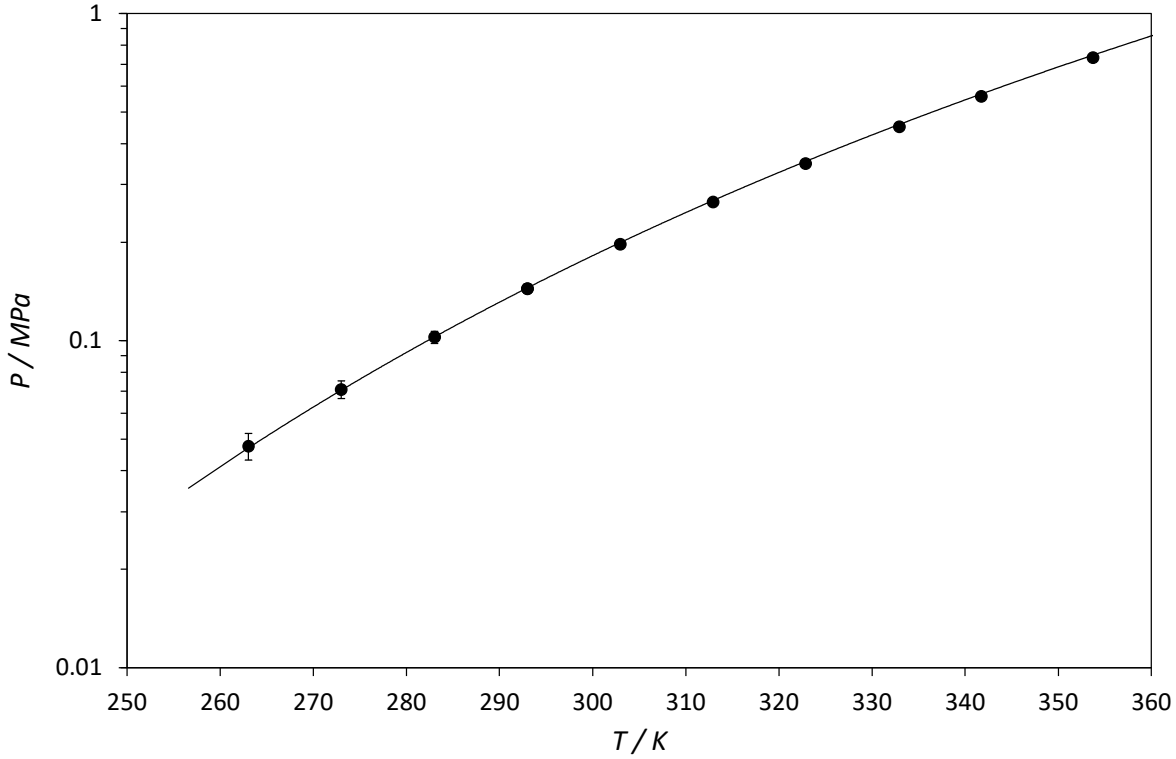

Figure 15. Comparison between measured VLE conditions of neo-pentane and its saturation line calculated from the reference equation of state, [1], from its triple-point temperature up to 360 K.
— : Ref. [1]; ● : measured value.

A similar comparison has not been performed for methane seeing that methane liquefies at temperatures lower the lowest achievable temperature of the thermo-regulated bath (about -70°C).

4.2 Procedure

The equilibrium cell and its loading lines are first evacuated at ambient temperature. The cell is then lowered into the thermo-regulated bath. The temperature of the cell is set to the target value by means of the temperature regulator, and adequate stirring is maintained throughout the cell.

For target temperatures higher than the triple-point temperature of neo-pentane (256.6 K), a certain amount of neo-pentane is introduced into the cell after stabilization of the Pt100 probes' signals at the target temperature. Some methane is then loaded in the cell until reaching the desired pressure at the target temperature.

For target temperatures lower than the triple-point temperature of neo-pentane, a certain amount of neo-pentane is introduced at about 273.15 K in order to avoid the solidification of neo-pentane in the loading line. Some methane is then introduced step-by-step into the cell in order to avoid solid deposition during the further cooling down to the target temperature.

At the target temperature, the phase equilibrium is assumed to be achieved when the pressure and temperature readings have stabilized to within their instrument uncertainty for at least 10 minutes. Once equilibrium is reached, sampling of the equilibrium phases starts while temperature and pressure readings are recorded. The liquid and vapor ROLSI® samplers are used for sampling the liquid phase and the vapor phase, respectively. The samples are then transferred to the GC and analyzed. The phase equilibrium is considered properly achieved once at least five/six repeatable molar compositions are obtained for both the liquid and the vapor phase.

Thereafter, some methane is added into the equilibrium cell and the process is repeated at a higher pressure and the same target temperature until the phase equilibrium behavior has been satisfactorily determined up to the critical-point region of the mixture.

4.3 Calculation of uncertainties

The approach adopted for estimating the experimental uncertainties is based on the NIST documentation by Taylor and Kuyatt [20]. Please refer to the Supplementary Material S2 for details related to the calculation of the uncertainties affecting the experimental results presented in this work.

Regardless of the nature of the quantity *M* being studied, the objective is to express an interval of uncertainty for *M* that is a combination of all the possible sources of uncertainties. This is referred to as the combined uncertainty, $u(M)$:

$$u(M) = \sqrt{\sum_i [u_i(M)]^2} \tag{7}$$

where $u_i(M)$ could be any source of uncertainty, such as errors resulting from the use of a calibration polynomial, or the standard deviation from averaging multiple observations.

There are three sources of uncertainties which are associated to an experimental value of temperature or pressure obtained as average of several records: (i) the uncertainty of the reference device (u_{REF}), (ii) the uncertainty that originates from the error related to the use of a calibration polynomial for calculating the true value of *M* (*T* or *p*) from the values measured by the instrument (u_{CAL}), and (iii) the uncertainty related to the repeatability of the measurement associated to the averaging of several records of M during an experiment (u_{REP}).

Four are the sources of uncertainties which are associated to an experimental value of molar composition: (i) the uncertainty related to the use of calibration polynomial for calculating the number of moles of each component in the mixture from the peaks of the gas-chromatograph (u_{CAL}), (ii) the uncertainty related to the purity of the chemicals (u_{PUR}), (iii) the uncertainty

resulting from the propagation of the errors when applying a mathematical formula for calculating the mole fractions from numbers of moles (u_{FOR}), and (iv) the uncertainty related to the repeatability of the measurements (u_{REP}).

To sum up, Table 6 gathers the uncertainties related to the uncertainty u_{REF} of the reference devices (reference platinum resistance thermometer and PACE 5000 modular pressure controller), the uncertainty u_{CAL} related to the use of calibration polynomials, the uncertainty u_{REP} related to the repeatability of the measurements, the uncertainty u_{FOR} related to the calculation of mole fractions from the number of moles of methane and neo-pentane, and to the uncertainty u_{PUR} related to the purity of the chemicals. These uncertainties affect the two experimental temperatures (obtained from the readings of the top and bottom Pt100 probes), the experimental pressure (obtained from the readings of either the low-pressure or high-pressure transducer depending on the system pressure), and the molar composition of the equilibrium phases.

Table 6. Summary of the uncertainties affecting the experimental results.
u_{REF} : uncertainties related to the use of reference devices for the calibration of temperature probes and pressure transducers
u_{PUR} : uncertainties related to the purity of the chemicals
u_{CAL} : uncertainties related to the use of calibration polynomials for obtaining experimental temperatures and pressures from temperature and pressure readings, and number of moles from surfaces of the GC's peaks
u_{FOR} : uncertainties related to the calculation of molar fractions from number of moles
u_{REP} : uncertainties related to repeatability of the experimental temperatures, pressures, and molar fractions

Uncertainty	Bottom Pt-100 probe	Top Pt-100 probe	Low-p transducer	High-p transducer	Molar fraction CH_4	Molar fraction neo-C_5H_{12}
u_{REF}	8 mK		0.09 kPa			
u_{CAL}*	9 mK	12 mK	0.23 kPa	1.04 kPa	0.4 µmol	5.8 µmol
u_{PUR}					29 µmol/mol	5.8 mmol/mol
u_{FOR}**					6 mmol/mol	
u_{REP}**	29 mK	32 mK	2 kPa	4 kPa	1.1 mmol/mol (y)	
					0.9 mmol/mol (x)	

*: for the molar fractions, the given u_{CAL} corresponds to the maximum uncertainties related to the use of the calibration polynomials for calculating the number of moles from the surfaces of the GC's peaks
**: maximum uncertainties related to the repeatability with respect to all the measured VLE

The purity of the chemicals used in this work affects the experimental fractions of the equilibrium phases with an uncertainty u_{PUR} of 29 μmol/mol (i = methane) and 5.8 mmol/mol (i = neo-pentane). These uncertainties are weighted by the number of moles of methane and neo-pentane sampled by means of the ROLSI® samplers, as detailed in the Supplementary Material S2. The maximum number of moles of methane and neo-pentane sampled during the experimental campaign are 36 μmol and 33 μmol, respectively.

The uncertainty accounting for the calibration of bottom Pt-100 probe and top Pt-100 probe is 9 and 12 mK, respectively. For the pressure transducers, u_{CAL} is 0.23 kPa (low-pressure transducer) and 1.04 kPa (high-pressure transducer). Provided that the uncertainties originating from the use of calibration polynomials for the calculation of the number of moles of methane and neo-pentane depend on the size of the GC's peaks the values of u_{CAL} gathered in Table 6 for the number of moles of the two components (0.4 and 5.8 μmol) are the maximum values encountered during the experimental campaigns carried out in this work.

The maximum values of the uncertainty related to the repeatability of the measurements of the different experimental values are shown in the 4th row of Table 6. Taking into account a total of about 1130 readings for each property (temperature, pressure, molar composition), the maximum uncertainties related to the repeatability are 29 mK for the bottom Pt-100 probe, 32 mK for the top Pt-100 probe, 2 kPa for the low-pressure transducer, 4 kPa for the high-pressure transducer, 1.1 mmol/mol for the molar fraction in the vapor phase, and 0.9 mmol/mol for the molar fraction in the liquid phase.

Once the combined uncertainty of each experimental quantity $u(M)$ has been calculated, a coverage factor k has been applied to obtain the expanded uncertainty, $U(M) = k \times u(M)$. The role of the coverage factor is to apply a particular confidence level by expanding the uncertainty

interval. In this work, a value of 2 has been chosen for k leading to a 95 % confidence level of the expanded uncertainty.

4.4 Critical-point estimation

The near-critical phase equilibrium behavior of the binary methane+neo-pentane mixture at the experimental temperatures investigated in this work has been estimated by applying the extended scaling laws presented in [21]. In particular, the critical-point pressure and composition at the experimental temperatures have been regressed taking into account a selected number of experimental vapor-liquid equilibria as detailed in Section 4.5.

At given temperature, the extended scaling laws proposed in [21] relate the compositions of one of the two components in the mixture (for instance methane, subscript 1) in the vapor (y_1) and liquid (x_1) phases at VLE in the near-critical region to the critical composition ($x_{C,1}$) and to the difference between the critical pressure (p_C) and the VLE pressure (p):

$$y_1 - x_1 = \lambda_1 (p_C - p) + \mu (p_C - p)^{0.325} \tag{8}$$

$$\frac{y_1 + x_1}{2} - x_{C,1} = \lambda_2 (p_C - p) \tag{9}$$

The combination of Eq. (8) and Eq. (9) yields:

$$x_1 = x_{C,1} + \left(\lambda_2 - \frac{\lambda_1}{2}\right)(p_C - p) - \frac{\mu}{2}(p_C - p)^{0.325} \tag{10}$$

$$y_1 = x_{C,1} + \left(\lambda_2 + \frac{\lambda_1}{2}\right)(p_C - p) + \frac{\mu}{2}(p_C - p)^{0.325} \tag{11}$$

In Eqs. (8)-(11), p_C, $x_{C,1}$, and the adjustable parameters (λ_1, λ_2, and μ) are regressed from a set of measured VLE points in the near-critical region at a given temperature. At a given temperature, the objective function (*fob*) is given by the sum of the percentage absolute errors between calculated (x_1 from Eq. (8) and y_1 from Eq. (9)) and experimental compositions of methane in the vapor and liquid phase ($x_{1,EXP}$ and $y_{1,EXP}$) of a selected number (N) of measured VLE:

$$fob = \sum_{i=1}^{N} 100 \times \left[\frac{\left| x_{1,i} - x_{1,EXP,i} \right|}{x_{1,EXP,i}} + \frac{\left| y_{1,i} - y_{1,EXP,i} \right|}{y_{1,EXP,i}} \right] \quad (12)$$

4.5 Results

The vapor-liquid equilibrium of the methane+neo-pentane system measured in this work are gathered in Table 7 (213 K < T < 243 K), Table 8 (253 K < T < 274 K), and Table 9 (298 K < T < 345 K). In each table, N_x and N_y are the number of repeatable samples (in terms of molar fraction) of the liquid and vapor phase, respectively.

Furthermore, VLE measurements have been listed according to their nominal temperature which represents the average of the corresponding experimental values. As indicated in Section 4.1, each experimental VLE temperature within Tables 7-9 is the average between the experimental temperatures of top Pt-100 probe and bottom Pt-100 probe; the difference between these temperatures has never exceeded 0.1 K.

Table 7. Experimental VLE of the (x_1)CH_4+(1-x_1)neo-pentane system from 213 K up to 243 K.
x_1 : molar composition of methane in the liquid phase; y_1 : molar composition of methane in the vapor phase; N_x: total number of repeatable samples of the liquid phase; N_y: total number of repeatable samples of the vapor phase; $U^{REL}(M)$: relative expanded (k=2) combined uncertainty of property M, $U^{REL}(M) = 2 \times u(M) / M$. For each nominal temperature, the VLE in the rows beyond the dashed line have been used in extended scaling laws presented in Ref. [21] for calculating the critical point of the mixture (shown in italic style).

T K	$U^{REL}(T)$ %	p MPa	$U^{REL}(p)$ %	N_x	x_1 mol/mol	$U^{REL}(x_1)$ %	N_y	y_1 mol/mol	$U^{REL}(y_1)$ %
Nominal temperature 212.59 K									
212.65	0.02	2.000	0.04	5	0.2702	2.81	5	0.9959	0.02
212.60	0.03	3.002	0.02	9	0.3987	2.39	6	0.9972	0.02
212.68	0.02	3.794	0.02	7	0.4977	2.03	6	0.9971	0.01
212.61	0.03	4.591	0.03	5	0.5966	1.72	5	0.9966	0.01
212.69	0.02	5.385	0.04	6	0.6928	1.35	7	0.9954	0.02
212.50	0.02	6.000	0.05	8	0.7727	0.98	6	0.9935	0.03
212.59	0.04	6.521	0.12	6	0.8451	0.67	8	0.9899	0.04
212.66	0.03	6.879	0.08	10	0.9021	0.40	5	0.9823	0.07
212.49	0.03	6.997	0.09	6	0.9347	0.28	5	0.9723	0.11
212.46	0.02	7.008	0.03	5	0.9416	0.24	5	0.9686	0.13
212.59		*7.020*			*0.9541*			*0.9541*	
Nominal temperature 230.20 K									
230.18	0.02	1.593	0.08	8	0.1713	3.51	7	0.9913	0.04
230.09	0.02	2.964	0.05	6	0.3113	2.97	8	0.9935	0.03
230.13	0.02	4.178	0.05	7	0.4253	2.40	16	0.9934	0.03
230.11	0.02	5.385	0.04	7	0.5329	1.86	6	0.9923	0.03
230.10	0.02	6.616	0.03	6	0.6369	1.43	7	0.9895	0.04
230.10	0.02	7.622	0.03	7	0.7216	1.09	6	0.9843	0.07
230.18	0.02	8.410	0.03	11	0.7925	0.83	13	0.9760	0.10
230.27	0.02	9.072	0.03	7	0.8684	0.53	8	0.9525	0.20
230.16	0.02	9.135	0.03	5	0.8830	0.47	5	0.9433	0.23
230.28	0.03	9.185	0.07	6	0.8928	0.44	5	0.9382	0.25
230.37	0.02	9.197	0.04	6	0.8961	0.43	7	0.9345	0.27
230.44	0.02	9.221	0.05	5	0.9042	0.40	5	0.9283	0.29
230.20		*9.232*			*0.9173*			*0.9173*	
Nominal temperature 242.97 K									
242.99	0.02	1.155	0.12	7	0.1067	4.01	6	0.9803	0.08
242.92	0.02	2.596	0.06	6	0.2378	3.52	6	0.9881	0.05
243.03	0.02	4.004	0.03	6	0.3546	2.68	5	0.9889	0.05
243.00	0.02	5.539	0.04	6	0.4741	2.19	6	0.9876	0.05
242.90	0.02	6.994	0.03	6	0.5765	1.66	6	0.9844	0.07
242.96	0.03	8.366	0.03	7	0.6736	1.33	6	0.9780	0.09
242.91	0.02	9.529	0.02	6	0.7606	1.00	6	0.9648	0.15
242.90	0.02	10.419	0.02	6	0.8504	0.65	8	0.9300	0.29
242.94	0.02	10.506	0.03	6	0.8718	0.54	6	0.9141	0.35
243.14	0.03	10.539	0.06	6	0.8822	0.55	5	0.9042	0.40
242.97		*10.549*			*0.8943*			*0.8943*	

Table 8. Experimental VLE of the (x_1)CH_4+(1-x_1)neo-pentane system from 253 K up to 274 K.
x_1 : molar composition of methane in the liquid phase; y_1 : molar composition of methane in the vapor phase; N_x: total number of repeatable samples of the liquid phase; N_y: total number of repeatable samples of the vapor phase; $U^{REL}(M)$: relative expanded (k=2) combined uncertainty of property M, $U^{REL}(M) = 2 \times u(M) / M$. For each nominal temperature, the VLE in the rows beyond the dashed line have been used in extended scaling laws presented in Ref. [21] for calculating the critical point of the mixture (shown in italic style).

T K	$U^{REL}(T)$ %	p MPa	$U^{REL}(p)$ %	N_x	x_1 mol/mol	$U^{REL}(x_1)$ %	N_y	y_1 mol/mol	$U^{REL}(y_1)$ %
Nominal temperature 253.34 K									
253.27	0.01	0.457	0.14				7	0.9161	0.41
253.34	0.01	0.781	0.18	8	0.0619	4.17	5	0.9517	0.21
253.33	0.01	2.525	0.12	8	0.2045	4.08	11	0.9809	0.08
253.36	0.01	4.066	0.05	7	0.3257	3.10	8	0.9836	0.07
253.31	0.01	5.634	0.06	7	0.4374	2.76	8	0.9828	0.08
253.33	0.02	7.200	0.03	5	0.5386	2.01	5	0.9794	0.09
253.32	0.02	8.684	0.02	5	0.6347	1.62	5	0.9721	0.14
253.34	0.01	10.117	0.02	5	0.7274	1.16	5	0.9546	0.19
253.38	0.02	11.142	0.02	6	0.8117	0.80	5	0.9249	0.39
253.39	0.02	11.333	0.03	5	0.8404	0.69	5	0.9094	0.37
253.34		*11.410*			*0.8774*			*0.8774*	
Nominal temperature 263.25 K									
263.24	0.01	0.476	0.17	6	0.0332	3.97	6	0.8848	0.47
263.25	0.02	1.027	0.13	7	0.0753	4.33	6	0.9453	0.22
263.24	0.02	2.631	0.12	6	0.1989	3.65	6	0.9718	0.12
263.26	0.01	3.982	0.05	6	0.2939	3.21	6	0.9740	0.12
263.26	0.01	5.731	0.06	6	0.4072	2.45	9	0.9738	0.11
263.23	0.01	7.559	0.06	9	0.5168	1.98	7	0.9703	0.14
263.23	0.01	9.165	0.04	9	0.6120	1.60	6	0.9607	0.18
263.23	0.01	10.253	0.03	7	0.6779	1.37	5	0.9499	0.25
263.25	0.01	11.326	0.02	7	0.7504	1.04	6	0.9292	0.30
263.24	0.01	11.905	0.02	7	0.8049	0.83	7	0.9029	0.39
263.34	0.02	12.046	0.04	5	0.8315	0.70	5	0.8792	0.48
263.25		*12.080*			*0.8590*			*0.8590*	
Nominal temperature 274.18 K									
274.36	0.03	1.004	0.05	8	0.0706	1.86	6	0.9136	0.17
274.22	0.01	2.022	0.06	8	0.1392	1.69	7	0.9512	0.10
274.24	0.01	3.756	0.06	8	0.2497	1.51	11	0.9641	0.07
274.21	0.01	5.512	0.04	6	0.3559	1.26	11	0.9659	0.07
274.14	0.01	7.600	0.27	6	0.4752	1.04	6	0.9620	0.08
274.22	0.01	9.520	0.22	5	0.5824	0.84	6	0.9513	0.10
274.22	0.02	11.575	0.18	6	0.7009	0.58	7	0.9202	0.16
274.25	0.01	12.287	0.16	6	0.7570	0.47	10	0.8929	0.21
274.00	0.01	12.503	0.16	6	0.7926	0.40	6	0.8680	0.27
273.97	0.01	12.541	0.16	11	0.8117	0.36	6	0.8582	0.28
274.18		*12.555*			*0.8333*			*0.8333*	

Table 9. Experimental VLE of the (x_1)CH_4+(1-x_1)neo-pentane system from 298 K up to 345 K.
x_1 : molar composition of methane in the liquid phase; y_1 : molar composition of methane in the vapor phase; N_x: total number of repeatable samples of the liquid phase; N_y: total number of repeatable samples of the vapor phase; $U^{REL}(M)$: relative expanded (k=2) combined uncertainty of property M, $U^{REL}(M) = 2 \times u(M) / M$. For each nominal temperature, the VLE in the rows beyond the dashed line have been used in extended scaling laws presented in Ref. [21] for calculating the critical point of the mixture (shown in italic style).

T K	$U^{REL}(T)$ %	p MPa	$U^{REL}(p)$ %	N_x	x_1 mol/mol	$U^{REL}(x_1)$ %	N_y	y_1 mol/mol	$U^{REL}(y_1)$ %
Nominal temperature 298.18 K									
298.18	0.01	0.811	0.07	8	0.0395	1.89	13	0.7652	0.45
298.16	0.01	1.502	0.06	18	0.0817	1.81	7	0.8610	0.27
298.19	0.01	3.236	0.10	6	0.1820	1.63	14	0.9171	0.17
298.18	0.02	6.048	0.33	7	0.3370	1.33	7	0.9315	0.14
298.20	0.01	9.042	0.22	7	0.4878	1.00	7	0.9240	0.17
298.21	0.01	11.873	0.17	6	0.6381	0.72	7	0.8860	0.23
298.21	0.01	12.577	0.16	7	0.6879	0.60	7	0.8612	0.28
298.20	0.02	12.856	0.16	6	0.7169	0.54	6	0.8414	0.31
298.21	0.01	12.951	0.15	6	0.7314	0.52	5	0.8296	0.34
298.20	0.01	12.994	0.15	10	0.7406	0.50	6	0.8156	0.37
297.99	0.02	13.024	0.16	7	0.7500	0.48	8	0.8055	0.39
298.18		*13.035*			*0.7830*			*0.7830*	
Nominal temperature 344.52 K									
344.52	0.01	0.981	0.06				6	0.3405	1.26
344.52	0.01	2.228	0.06	6	0.0859	1.76	7	0.6608	0.65
344.51	0.01	4.031	0.04	6	0.1742	1.60	6	0.7698	0.45
344.53	0.01	6.047	0.33	7	0.2696	1.41	9	0.8048	0.40
344.51	0.01	8.038	0.25	6	0.3682	1.22	5	0.8086	0.39
344.53	0.01	10.204	0.20	9	0.4784	1.03	6	0.7858	0.44
344.52	0.01	11.098	0.18	9	0.5351	0.93	6	0.7593	0.49
344.51	0.01	11.641	0.17	6	0.5874	0.83	7	0.7202	0.56
344.52	0.01	11.741	0.17	7	0.6059	0.80	6	0.7037	0.60
344.52	0.01	11.775	0.17	7	0.6169	0.78	6	0.6893	0.62
344.52		*11.810*			*0.6566*			*0.6566*	

For each nominal temperature, the VLE in the rows below the horizontal dashed line have been used for the calculation of the near-critical point behavior, and the calculated critical coordinates (critical pressure and critical composition) are shown in italic style in the last row of the corresponding nominal temperature.

The maximum expanded (k=2) combined uncertainty (U^{REL}) on the experimental temperature (0.04%) is found for the 7th VLE point at the nominal temperature of 212.59 K: the corresponding absolute values is U = 94 mK. With respect to pressure, the maximum U^{REL} is

0.33% and it affects the pressure of the 4th VLE point at the nominal temperature of 344.52 K; the corresponding absolute values is U = 20 kPa.

The maximum U^{REL} affecting the molar composition of the equilibrium phases are 1.26% (vapor phase of the 1st VLE point at the nominal temperature of 344.52 K) and 4.33% (liquid phase of the 2nd VLE point at the nominal temperature of 263.25 K).

The experimental VLE gathered in Tables 7-9 are shown in Figure 16 (213 K < T < 253 K) and in Figure 17 (263 K < T < 345 K).

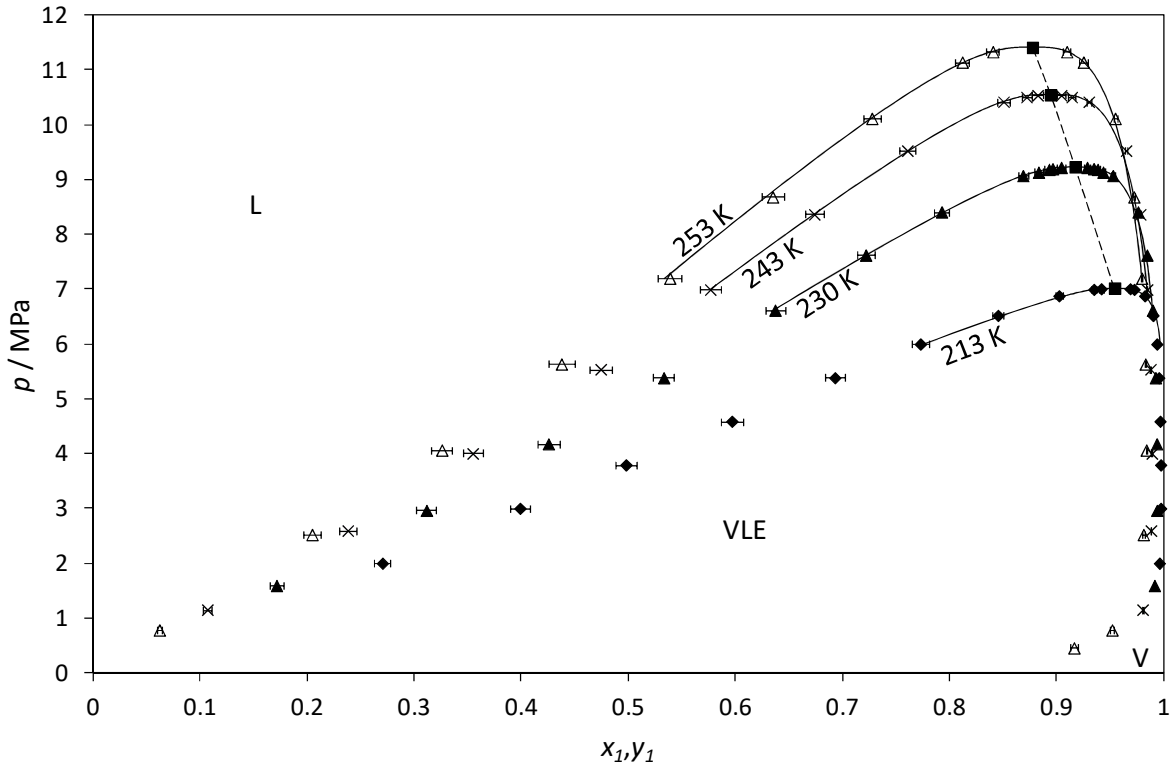

Figure 16. Experimental VLE data from 213 K up to 253 K for the (1)CH_4+(2)neo-C_5H_{12} system.

♦ : 212.59 K; ▲ : 230.20 K; × : 242.97 K; Δ : 253.34 K; — : near-critical phase equilibrium behavior calculated following the extended scaling laws; – – : calculated critical locus of the mixture; ■ : calculated critical point of the mixture.

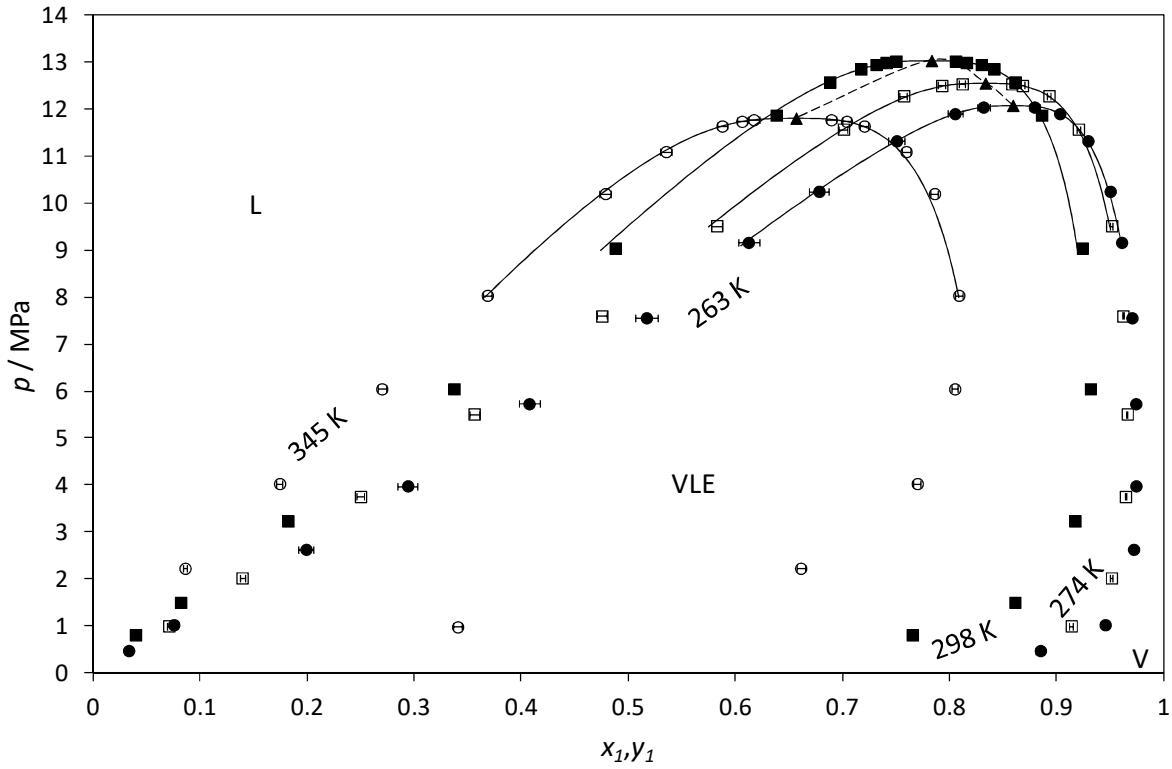

Figure 17. Experimental VLE data from 263 K up to 345 K for the (1)CH_4+(2)neo-C_5H_{12} system.

● : 263.25 K; □ : 274.18 K; ■ : 298.18 K; ○ : 344.52 K; — : near-critical phase equilibrium behavior calculated following the extended scaling laws; – – : calculated critical locus of the mixture; ▲ : calculated critical point of the mixture.

In Figures 16 and 17, the continuous lines represent the near-critical phase equilibrium behavior as calculated by means of the extended scaling laws, whereas the dashed lines join the calculated critical points. The experimental VLE in terms of relative volatility and in the whole temperature range are also illustrated and compared to the calculated near-critical phase equilibrium behavior in Figure 18.

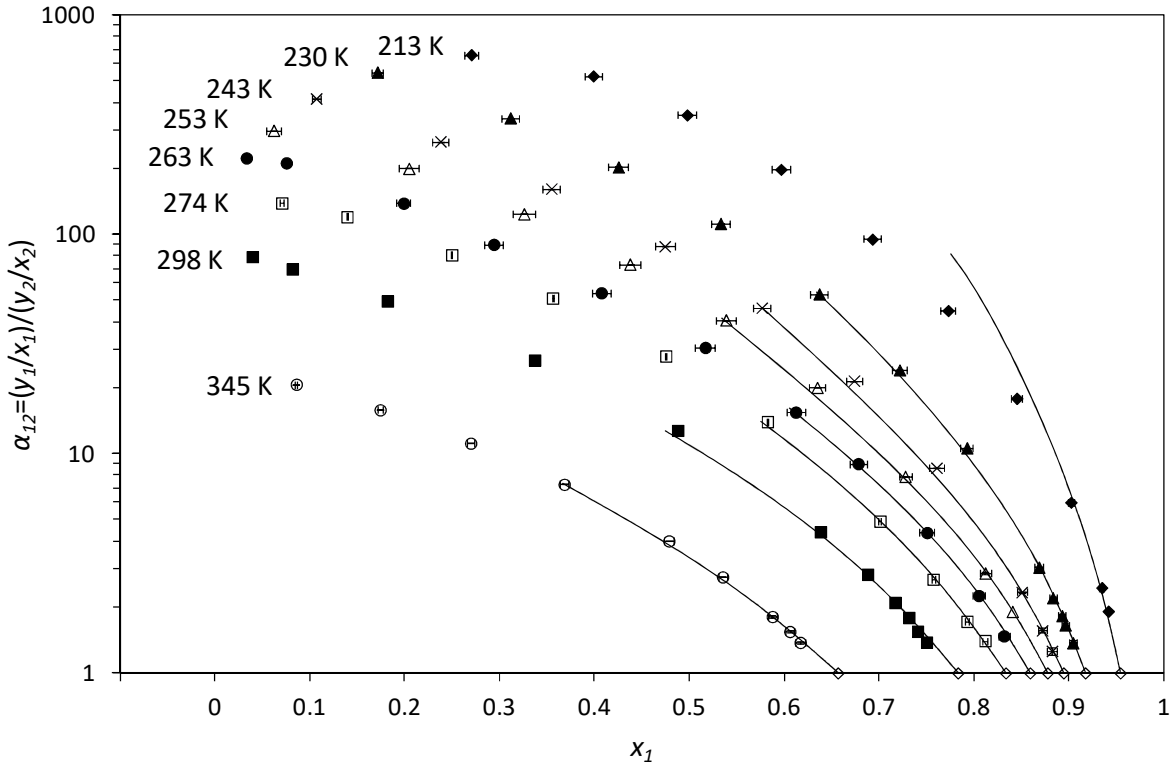

Figure 18. Relative volatility of the (1)CH_4+(2)neo-C_5H_{12} system from 213 K up to 345 K.

♦ : 212.59 K; ▲ : 230.20 K; × : 242.97 K; Δ : 253.34 K; ● : 263.25 K; □ : 274.18 K; ■ : 298.18 K; ○ : 344.52 K — : near-critical phase equilibrium behavior calculated following the extended scaling laws; ◊ : calculated critical point of the mixture.

Please refer to the Supplementary Material S3 for details concerning the values of the parameters of the extended scaling laws (λ_1, λ_2, and μ) together with an analysis about their variation with temperature related to the form of the vapor-liquid equilibrium measured in this work.

The PPR78 and PSRK EoSs have been applied and compared to the literature VLE and the experimental VLE at 298 K and 345 K.

Figure 19 illustrates the comparison between the two predictive models, literature values from Ref. [7], and the experimental values at nominal temperature 298.18 K gathered in Table 9. The experimental compositions of the liquid phase presented in Ref. [7] and the ones presented in this work are in a quite good agreement at least up to the critical region (P < 12 MPa). To the

contrary, the vapor phase at VLE from Ref. [7] is richer in methane than the one presented in this work.

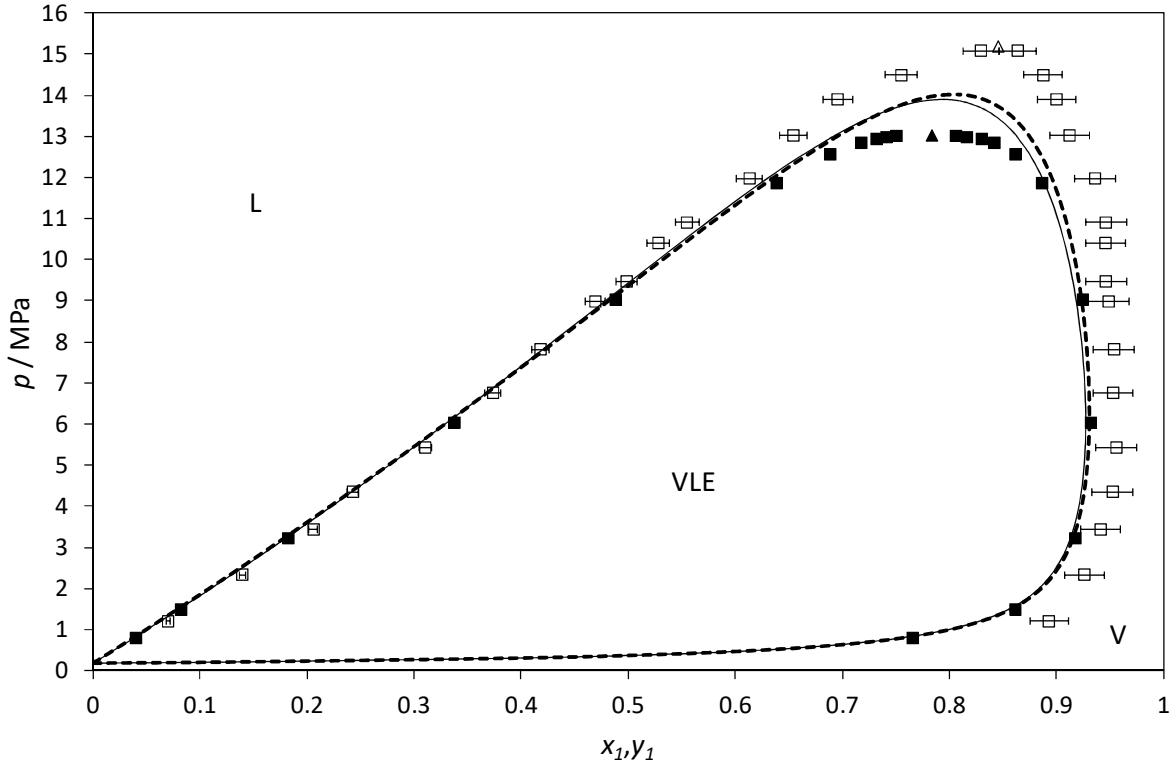

Figure 19. Comparison between predicted VLE, literature data, and experimental data at 298 K.

VLE: literature values from Ref. [7] (□); experimental values, this work (■), PPR78 EoS (—); PSRK EoS (– –). Critical points: literature value from Ref. [7] (Δ); extended scaling laws, this work (▲).

Figure 20 illustrates the comparison between the PSRK EoS (similar results are obtained when the PPR78 EoS is used), literature values from Ref. [6] from 344.26 K up to 410.93 K, and the experimental values at nominal temperature 344.52 K gathered in Table 9. A good agreement between the two sets of VLE data (Ref. [6] and this work) at 345 K is observed for both the equilibrium phases.

To sum up, it can be stated that the VLE predictions agree with the VLE measured in this work at the two temperatures. Meanwhile, the VLE calculated by means of the PPR78 and PSRK EoSs do not agree neither with the data presented in Ref. [7] (Figure 19) nor with the data

(especially the compositions of the vapor phase) presented in Ref. [6] at 377.59 K and 410.93 K (Figure 20).

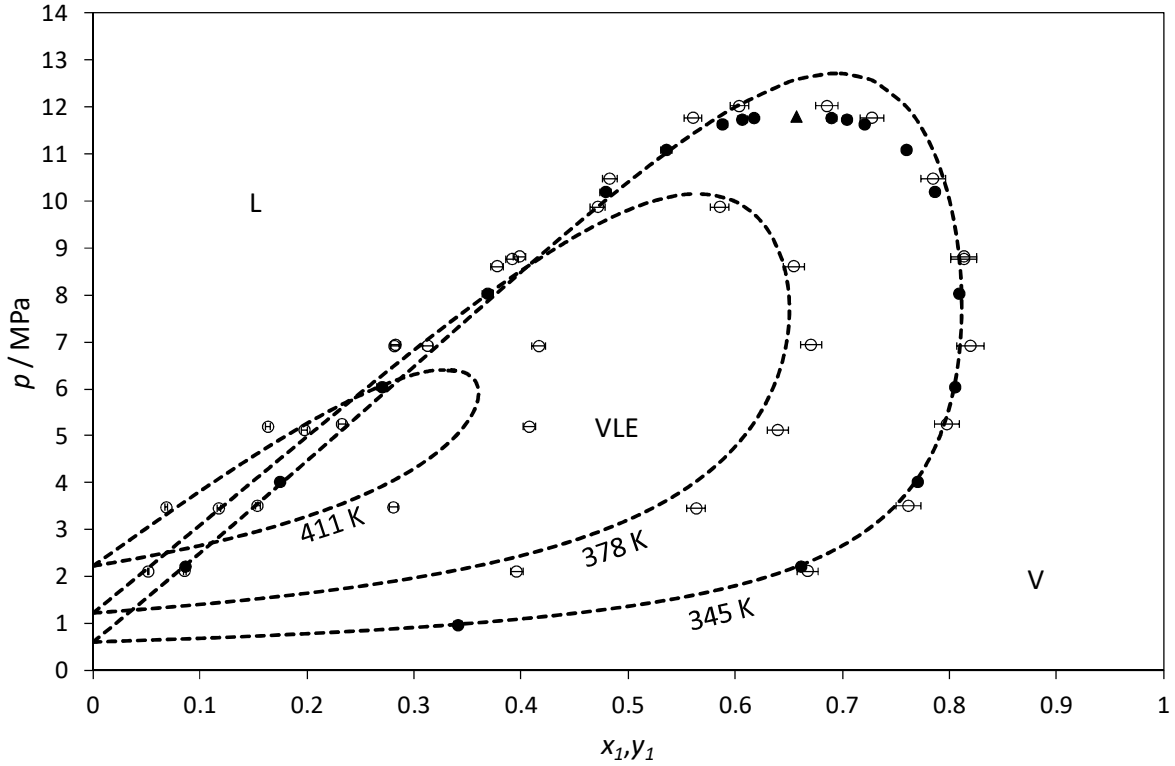

Figure 20. Comparison between predicted VLE, literature data, and experimental data at 345 K, 378 K, and 411 K.

VLE: literature values from Ref. [6] at 344.26 K, 377.59 K, and 410.93 K (○); experimental values at 344.52 K, this work (●), PSRK EoS (– –). Critical point: extended scaling laws, this work (▲).

5. Global phase equilibrium behavior from PR EoS with regressed k_{ij}

The phase equilibrium measurements presented in Tables 7-9 for the system methane+neo-pentane are a solid evidence of the existence of the vapor-liquid equilibrium at temperatures lower than the triple-point temperature of neo-pentane, at least down to about 213 K.

The VLE measured in this work endorse then the phase equilibrium behavior of the binary mixture as predicted by the PPR78 and PSRK EoSs (coupled with the Classical Approach for solid methane and neo-pentane) and are not in agreement with the solid-vapor equilibria presented in Ref. [8].

In this section, the Peng-Robinson Equation of State (PR EoS), [22], (as implemented in Simulis Thermodynamics Software, [17]) has been applied for calculating the global phase equilibrium behavior of the methane+neo-pentane system. Modeling results have been then compared to literature VLE and SVE (see Table 2), and VLE presented in this work.

5.1 Thermodynamic framework

For the reader convenience, the functional form of the PR EoS, mixing rules for the attractive parameter (a) and covolume (b), and attractive term (a_i) and covolume (b_i) of the i^{th}-component in the mixture of N_C components are reminded here below.

$$p = \frac{RT}{v-b} - \frac{a}{v^2 + 2bv - b^2} \tag{13}$$

$$a = \sum_{i=1}^{N_C}\sum_{j=1}^{N_C} x_i x_j \left(1 - k_{ij}\right)\sqrt{a_i a_j} \tag{14}$$

$$b = \sum_{i=1}^{N_C} x_i b_i \tag{15}$$

$$a_i = 0.45724\frac{(RT_C)^2}{P_c}\left[1 + (0.37464 + 1.54226\omega_i - 0.26992\omega_i^2)\left(1 - \sqrt{\frac{T}{T_C}}\right)\right]^2 \tag{16}$$

$$b_i = 0.07780\frac{RT_C}{P_c} \tag{17}$$

The application of the PR EoS to the calculation of fluid-phase equilibrium properties to be coupled with the fugacity of solid neo-pentane, Eqs. (5)-(6), for the representation of the global phase equilibrium behavior of the binary mixture has been based on the regression of the binary interaction parameter (k_{ij}) with respect to literature VLE and values measured in this work.

5.2 Approach

For each VLE temperature (T_j), the Objective Function (OF) that has been used in the regression of k_{ij} considers the absolute relative deviation between the experimental molar compositions of methane (1) and neo-pentane (2) in the equilibrium phases ($x_{1,2}^{EXP}$ and $y_{1,2}^{EXP}$) and the molar compositions calculated by the PR EoS via a FLASH calculation ($x_{1,2}^{CALC}$ and $y_{1,2}^{CALC}$).

$$OF(T_j) = 100\left\{\sum_{i=1}^{2}\left[\frac{\left|x_i^{EXP} - x_i^{CALC}\right|}{x_i^{EXP}} + \frac{\left|y_i^{EXP} - y_i^{CALC}\right|}{y_i^{EXP}}\right]\right\} \quad (18)$$

In the FLASH calculation, experimental temperatures and pressures have been imposed as input values together with global compositions calculated as the average between the experimental VLE compositions.

The regressed values of the binary interaction parameter of the methane+neo-pentane system are illustrated in Figure 21.

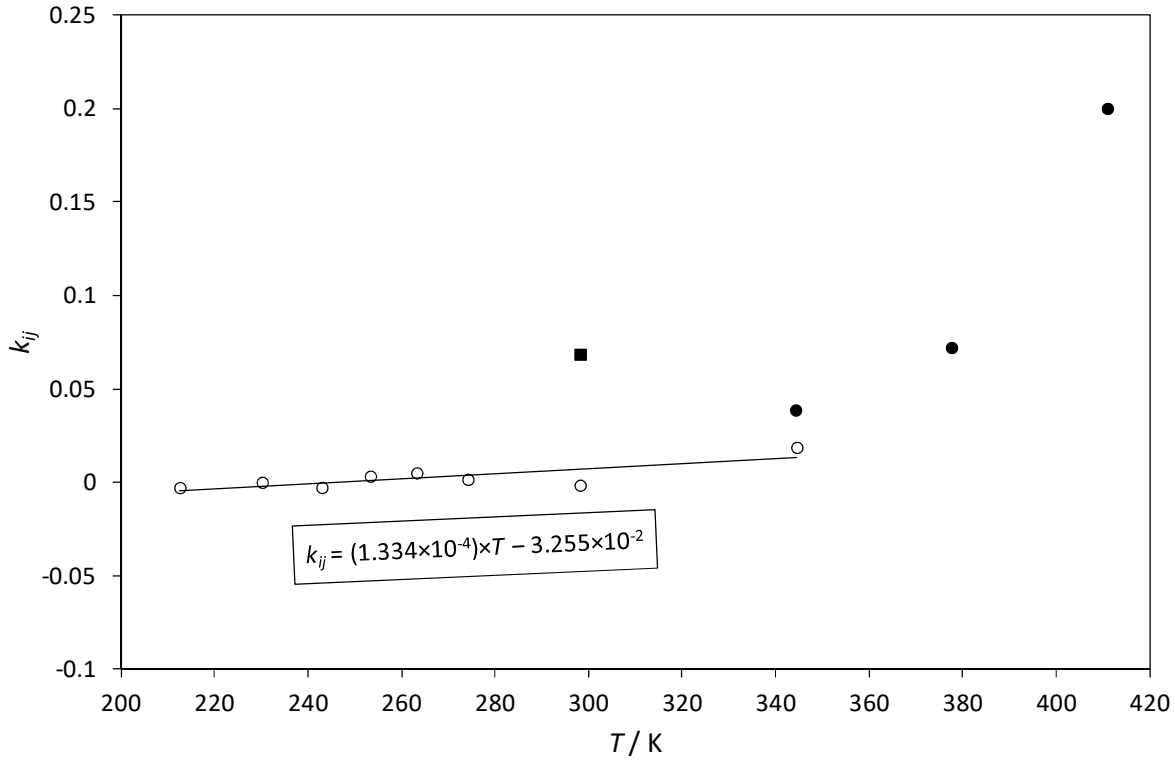

Figure 21. Regressed binary interaction parameter of the CH_4+neo-C_5H_{12} system as function of the system temperature.
Corresponding VLE: Ref. [6] (●); Ref. [7] (■); this work (○).

In Figure 21, filled circles are related to the VLE presented in Ref. [6], the filled square is related to the VLE presented in Ref. [7], whereas the open circles shown the values regressed with respect to the VLE presented in this work.

Taking into account the VLE measured in this work, k_{ij} appears to linearly increase for increasing temperatures from 213 K up to 345 K. A value of about 0.07 has been obtained at 298 K with respect to the VLE presented in Ref. [7]. This value differs from the value obtained with respect to the VLE gathered in Table 9 (about -0.0015) and it has been noticed that no value of k_{ij} between -0.1 and 0.1 allows a quantitative representation of the vapor phase given in Ref. [7]. Similarly, the k_{ij} regressed on the data of Ref. [6] at 377.59 K (0.072) and 410.93 K (0.2) deviates from the linear dependence that can be inferred from the open circles in Figure 21. The values regressed on the data of Ref. [6] allow the quantitative representation of the

experimental liquid phase but, as observed for the data of Ref. [7], no value of k_{ij} between -0.1 and 0.1 allows the simultaneous quantitative representation of the vapor phase.

A higher polynomial function which could have been obtained by considering also the k_{ij} corresponding to the data of Ref. [6] would have probably lead to improper values (depending on the order of the polynomial) in the low temperature region. As a consequence, in the context of this work the linear temperature-dependence of k_{ij} obtained from the values regressed on the VLE gathered in Tables 7-9 has been used for predicting the phase equilibrium behavior at temperatures higher than 345 K and lower than 213 K. This first-order polynomial, also shown in Figure 21, is:

$$k_{ij} = (1.334 \times 10^{-4}) \times T - 3.255 \times 10^{-2} \quad (19)$$

Seeing that a very similar number of experimental points (from 9 to 12) has been measured for each isotherm presented in this work, fitting the different isotherms simultaneously by substituting k_{ij} for the first-order polynomial of temperature has given the same coefficients of Eq. (19).

5.3 Results

The qualitative comparison between the model (PR EoS with k_{ij} from Eq. (19)) and VLE measured in this work is shown in Figure 22 (213 K < T < 253 K) and in Figure 23 (263 K < T < 345 K).

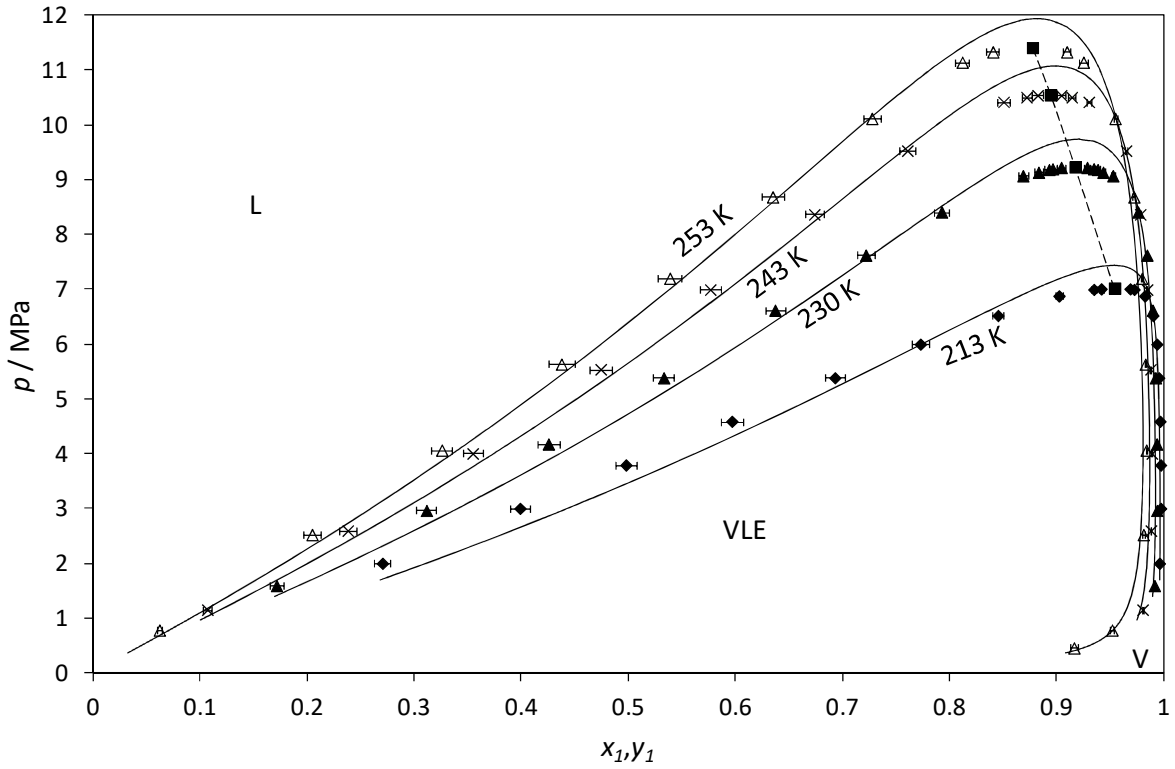

Figure 22. Pressure-composition phase equilibrium behavior at 213 K, 230 K, 243 K and 253 K for the (1)CH_4+(2)neo-C_5H_{12} system.

VLE: ♦ : 212.59 K; ▲ : 230.20 K; × : 242.97 K; Δ : 253.34 K; — : PR EoS. Values calculated via the extended scaling laws: critical locus of the mixture (– –) and critical point of the mixture (■).

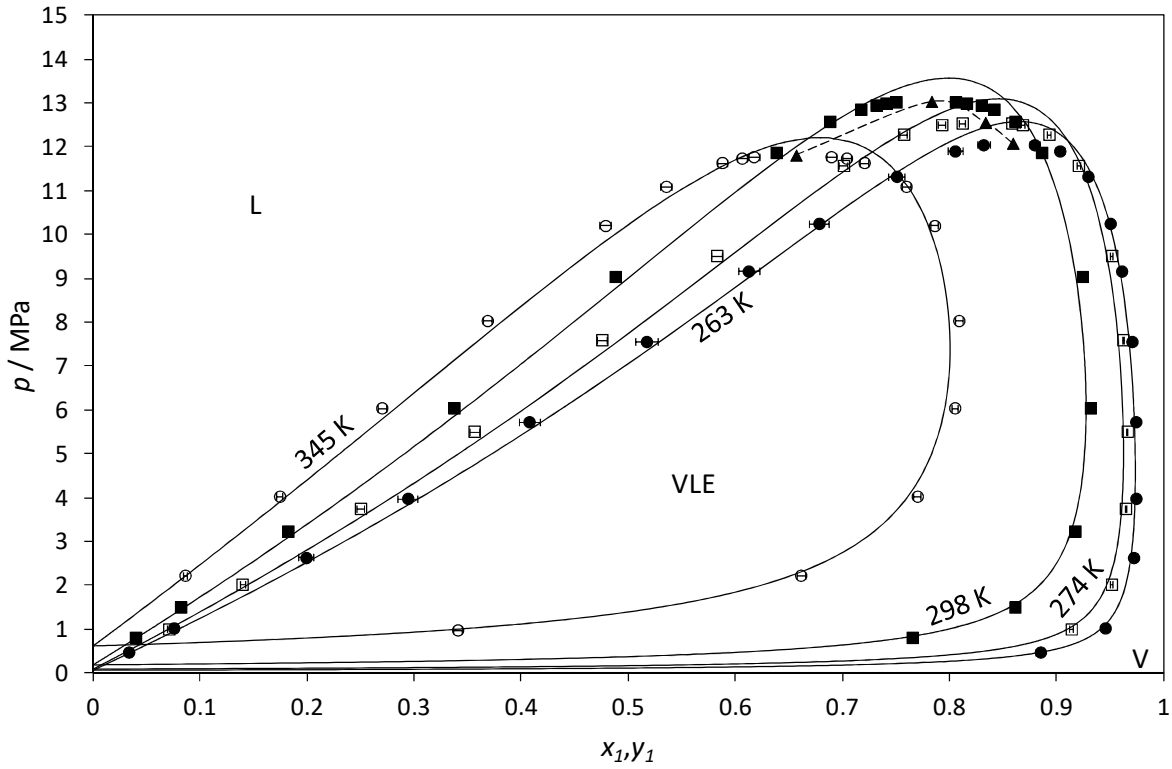

Figure 23. Pressure-composition phase equilibrium behavior at 263 K, 274 K, 298 K and 345 K for the (1)CH_4+(2)neo-C_5H_{12} system.

VLE: ● : 263.25 K; □ : 274.18 K; ■ : 298.18 K; ○ : 344.52 K; — : PR EoS. Values calculated via the extended scaling laws: critical locus of the mixture (– –) and critical point of the mixture (▲).

In Figures 22-23, continuous lines represent the modeling results. Contrary to Figure 23, in Figure 22 it is worth highlighting that the continuous lines do not reach the left y-axis (x_1,y_1=0) seeing that pure neo-pentane does not exhibit a saturation pressure at the temperatures of the pressure-composition phase equilibrium behaviors (these temperatures are lower that the triple-point temperature of neo-pentane). Unless for the critical-point region, there is a good agreement between the experimental VLE measured in this work and the modeling results, for both the vapor and the liquid phases.

In Figure 24, the comparison is shown for the VLE at 298 K. As observed in Figure 19 for the PPR78 and PSRK EoSs, the PR EoS with k_{ij} from Eq. (19) is not suitable for representing the data from Ref. [7].

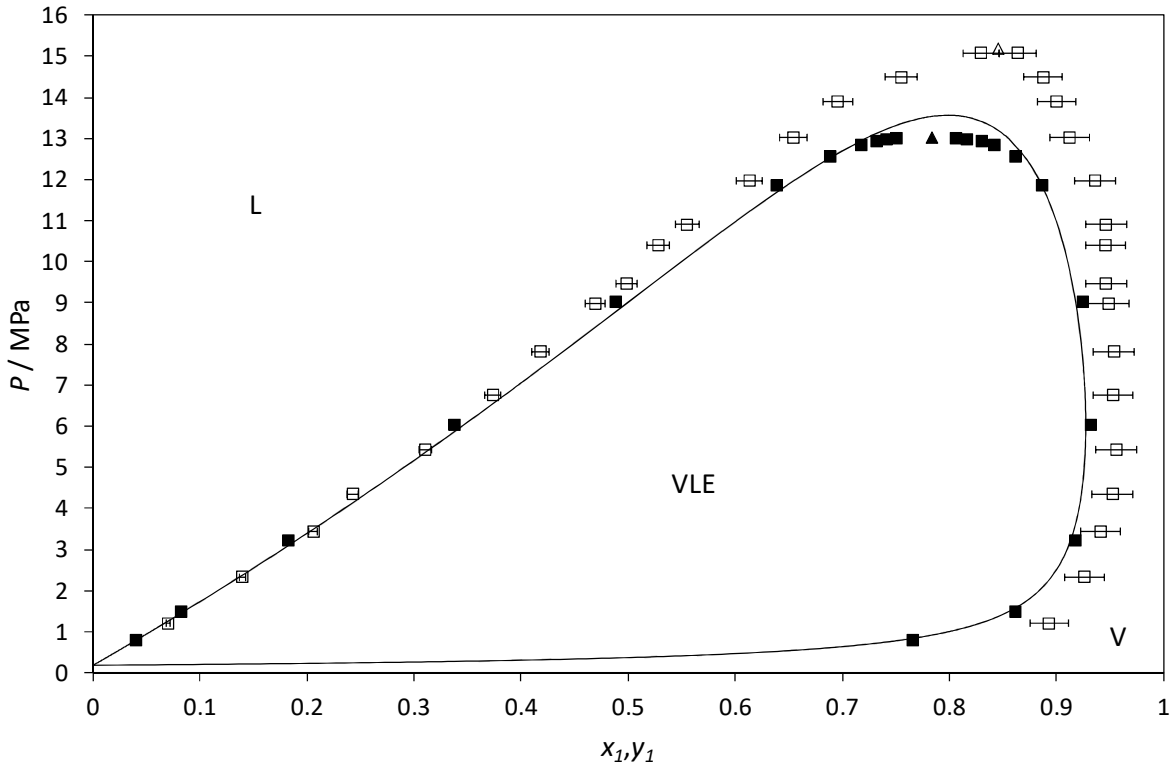

Figure 24. Pressure-composition phase equilibrium behavior at 298 K for the (1)CH_4+(2)neo-C_5H_{12} system.
Ref. [7] (□); this work (■,▲); — : PR EoS.

In Figure 25, the comparison is shown for the VLE at 345 K, 378 K, and 411 K. Because of the use of Eq. (19) rather than a higher-order polynomial (see Figure 21), higher deviations occur for both the liquid and the vapor phases at 378 K and 411 K than at 345 K. As discussed in Section 5.2, even the use of optimal k_{ij} at 378 K and 411 K does not allow a precise representation of the VLE data from Ref. [7], then the functional form of the PR EoS seems to be not suitable for the representation of the VLE of the methane+neo-pentane system in the high-temperature region (T > 350 K).

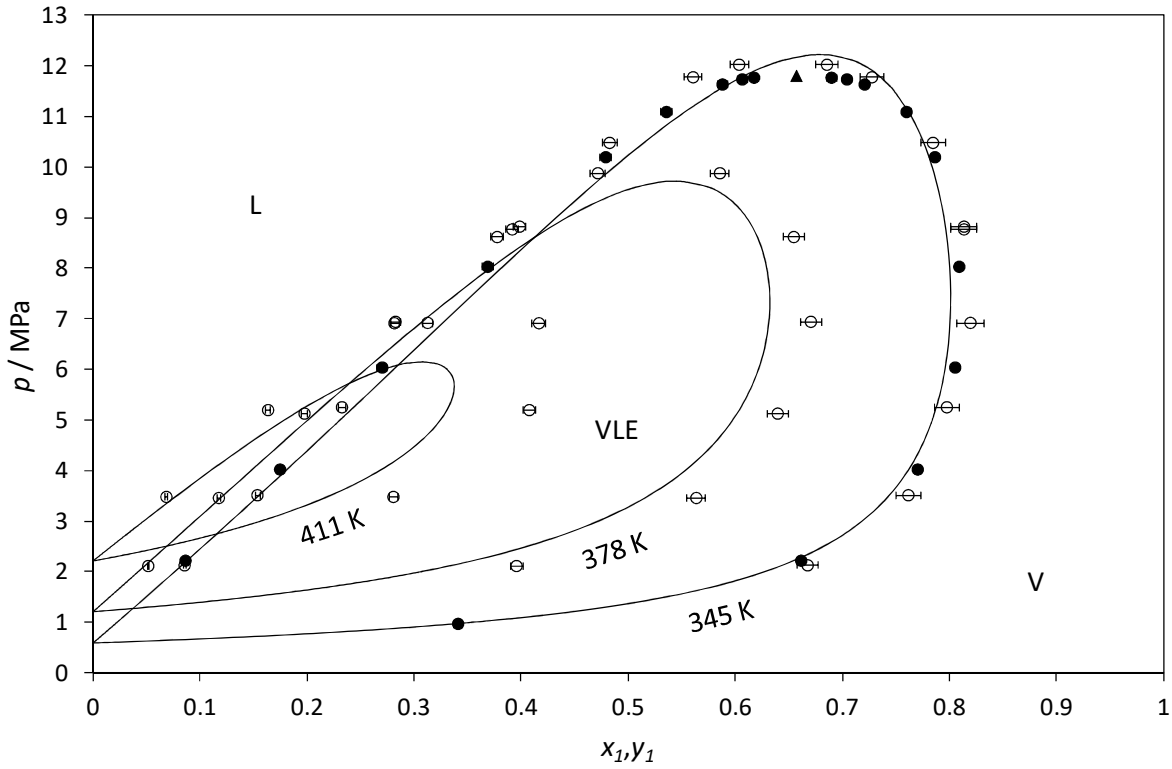

Figure 25. Pressure-composition phase equilibrium behavior at 345 K, 378 K, and 411 K for the (1)CH_4+(2)neo-C_5H_{12} system.
Ref. [6] (○); this work (●,▲); — : PR EoS.

Figure 26 illustrates the comparison between experimental (this work and values from Ref. [6]) and calculated relative volatilities. Except some points at 213 K and 243 K at low methane contents, a good quantitative comparison is observed between the relative volatility calculated from the VLE compositions given in Tables 7-9 and values obtained by means of the PR EoS. Higher deviations are obtained at 378 K and 411 K since the functional form of the binary interaction parameter, Eq. (19), has been obtained without considering the optimal k_{ij} at these temperatures. Nevertheless, the calculated relative volatility qualitatively agrees with the values calculated from the experimental VLE compositions presented in Ref. [6].

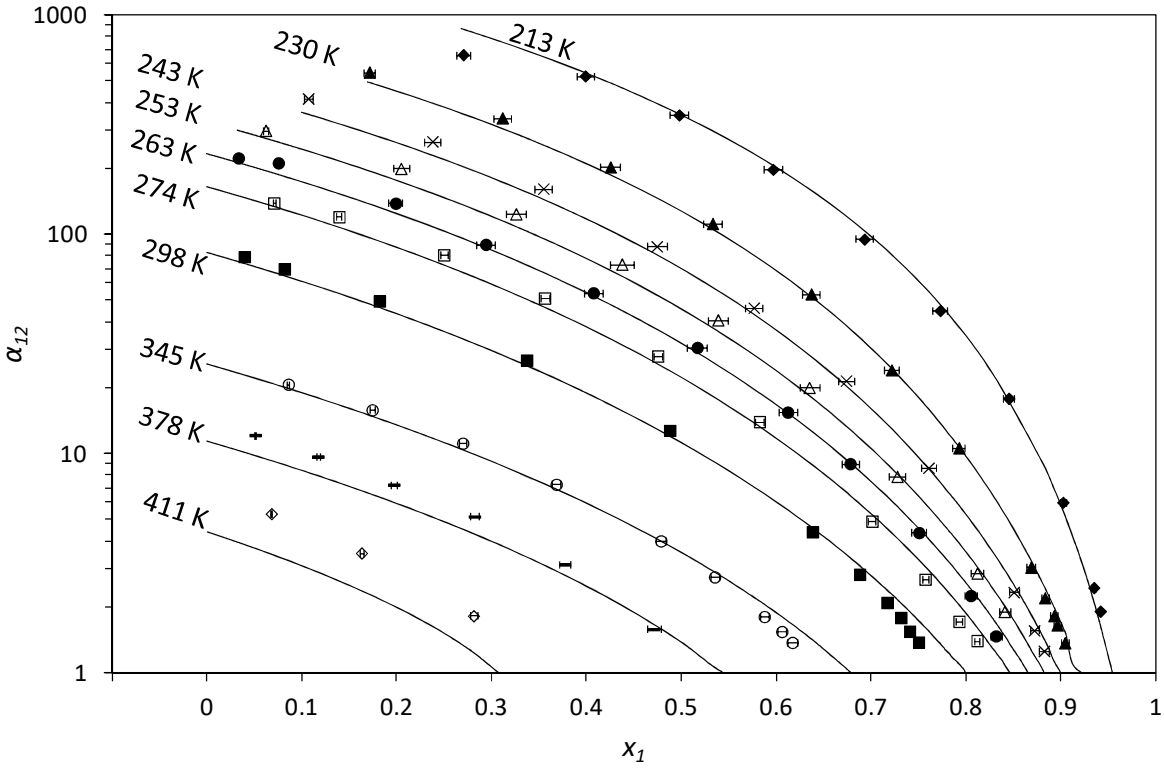

Figure 26. Relative volatility of the (1)CH_4+(2)neo-C_5H_{12} system from 213 K up to 411 K.

♦ : 212.59 K; ▲ : 230.20 K; × : 242.97 K; Δ : 253.34 K; ● : 263.25 K; □ : 274.18 K; ■ : 298.18 K; ○ : 344.52; ▬ : 377.59 K [6]; ◊ : 410.93 K [6]; — : PR EoS.

The quantitative comparison between all the VLE data and modeling results obtained thanks to the PR EoS with k_{ij} from Eq. (19) is gathered in Table 10.

Table 10. Quantitative comparison between experimental and calculated VLE values of the (1)methane+(2)neo-pentane system.

Ref.	*T* K	*N*	*N**	Errors in x_1			Errors in y_1		
				AAD%	*Bias%*	*MAD%*	*AAD%*	*Bias%*	*MAD%*
[6]	344.26	9	9	5.38	4.89	8.31	2.19	-0.83	4.91
	377.59	6	5	6.35	4.10	9.74	8.23	-8.23	15.74
	410.93	3	2	16.14	16.14	19.14	20.33	-20.33	21.86
Overall		18	16	7.02	6.05	19.14	6.35	-5.58	21.86
[7]	298.15	16	13	5.05	4.54	10.89	3.94	-3.94	6.88
This work	212.59	10	10	6.10	2.42	15.01	0.39	0.39	1.72
	230.20	12	12	4.98	0.69	11.87	1.15	1.09	3.70
	242.97	10	10	4.75	1.67	11.26	1.10	0.89	4.48
	253.34	10	10	4.47	2.99	14.31	0.64	0.37	2.46
	263.25	11	11	4.10	2.66	11.24	0.72	0.51	3.99
	274.18	10	10	3.20	1.55	5.57	1.23	0.77	4.60
	298.18	11	11	3.10	1.49	6.40	1.83	1.41	6.08
	344.52	10	10	2.93	2.45	4.98	2.03	0.86	6.59
Overall		84	84	4.21	1.96	15.01	1.14	0.80	6.59

The comparison has been done with respect to the percentage error $err_i\%$ and the percentage deviations: Absolute Average Deviation (AAD), Bias, and Maximum Absolute Deviation (MAD). $err_i\%$, *AAD%*, *Bias%*, and *MAD%* are defined as in Eqs. (20)-(23) with respect to a generic quantity *M* (molar composition of either the liquid or the vapor phase) and the total number N^* of calculated values (which can be different from the total number *N* of experimental values because of the representation of the critical region by the model).

$$err_i\% = 100 \times \left(\frac{M^{CALC} - M^{EXP}}{M^{EXP}} \right) \tag{20}$$

$$AAD\% = \frac{1}{N^*} \sum_{i=1}^{N^*} |err_i\%| \tag{21}$$

$$Bias\% = \frac{1}{N^*} \sum_{i=1}^{N^*} err_i\% \tag{22}$$

$$MAD\% = max\{|err_i\%|\} \quad (23)$$

In Table 10, the AAD%, Bias%, and MAD% are given for each experimental temperature of Ref. [6], Ref. [7], and this work; the total number N of data is in the third column, the number N^* of calculated VLE is in the fourth column, the errors related to the methane compositions in the liquid phase are listed from the 5th to 7th columns, and the errors related to the methane composition in the vapor phase are listed in the last three columns.

In Table 10, the overall rows summarize the quantitative comparisons between modeling results and VLE data from Ref. [6] and data presented in this work by combining the errors at each temperature. The overall errors have been calculated considering the number N^* of calculated values: the AAD and the Bias are the mathematical averages among the errors of all the experimental temperatures of the same reference, whereas the MAD is the highest value considering all the temperatures of the same reference.

With regard to Ref. [6], it is possible to confirm what has been previously discussed by observing Figure 25: the higher the VLE temperature (from 344.26 K up to 410.93 K), the higher the errors. As it can be seen in the overall row, the PR EoS with k_{ij} from Eq. (19) systematically overestimates the methane-content in the liquid phase (both AAD and Bias are positive and quite similar in value) and underestimates the methane-content in the vapor phase (the absolute value of the Bias is close to the AAD). In addition to that, a value close to 20% is obtained for the MAD of the methane-content in both the vapor and liquid phases.

Lower deviations are encountered for VLE data of Ref. [7] than the ones in the overall line for VLE data of Ref. [6], even though the deviations occurring at 298.15 K with respect to the data of Ref. [7] have the same order of magnitude of the deviations occurring at 344.26 K with respect to the data of Ref. [6].

Among all the errors given in Table 10, the lowest occur with respect to the VLE data presented in this work due to the fact that the temperature-dependent function, Eq. (19), has been obtained

by considering only the k_{ij} regressed on the data in Tables 7-9. The overall AAD is lower than 5% and 2% for the liquid and vapor phase, respectively. The model developed in this work slightly overestimates the methane-content of both the liquid and vapor phases (positive Bias, about 2% for the liquid phase, less than 1% for the vapor phase). The maximum MAD for the liquid phase (15.01%) occurs at the lowest VLE pressure at 212.59 K (which can be inferred from the mismatch between the calculated and experimental relative volatilities shown in Figure 26), whereas the maximum MAD for the vapor phase (6.59%) occurs at the highest VLE pressure at 344.52 K (11.741 MPa) and it is related to the deviation of the model with respect to experimental values in the critical region.

5.4 Discussion

The 6 isotherms published in Ref. [8] extend from 200 K up to 257.9 K and the corresponding equilibrium values have been associated to the solubility of solid neo-pentane in vapor (or supercritical) methane.

The highest temperature of the measurements in Ref. [8] is higher than the triple-point temperature of neo-pentane from Ref. [1] (256.6 K). Eq. (19) has been used in the mixing rules of the PR EoS, and the model has been applied at 257.9 K. Figure 27 shows the comparison between the VLE calculated by the model up to 10 MPa and the vapor composition of methane at S_2VE given in Ref. [8]. It is worth observing that the line representing the composition of the vapor phase at the calculated VLE is in a quite good agreement with the data of Ref. [8], and that these latter have not been used in the regression of the binary interaction parameters since in the same Ref. [8] they are presented as vapor composition at equilibrium with solid neo-pentane rather than a neo-pentane-rich liquid phase.

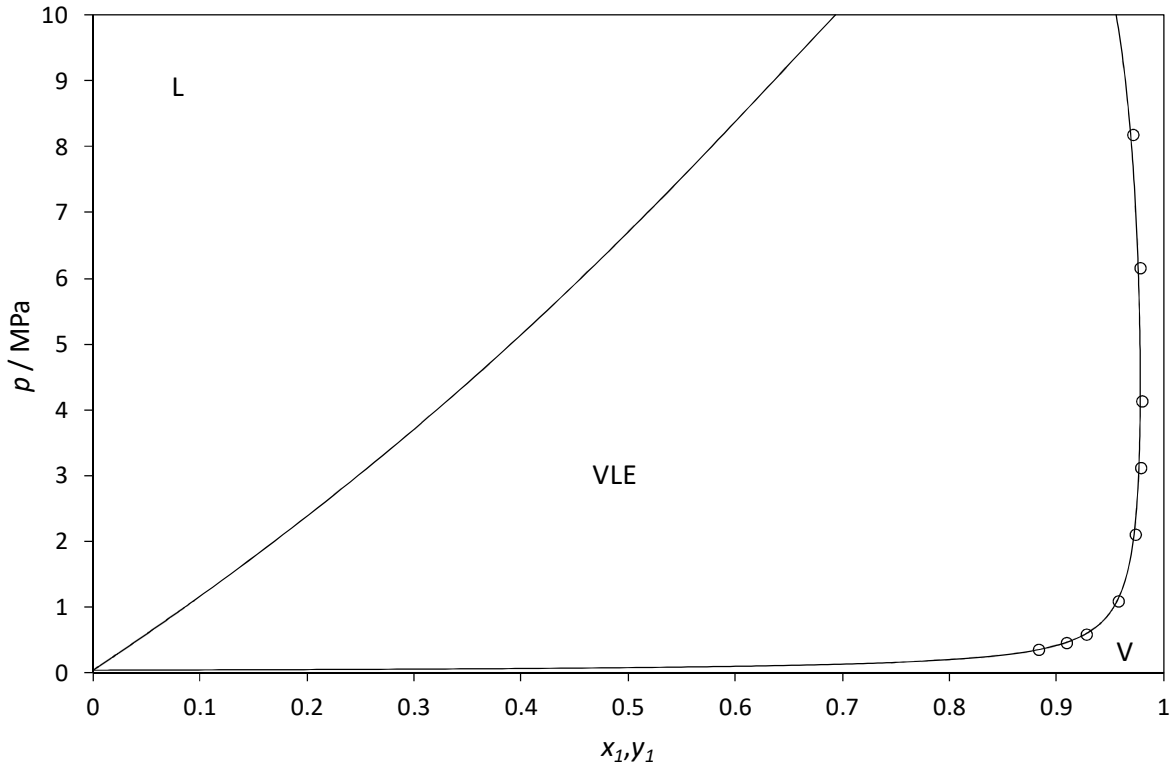

Figure 27. Pressure-composition phase equilibrium behavior at 257.9 K for the (1)CH_4+(2)neo-C_5H_{12} system.
○ : vapor compositions at S_2VE from Ref. [8]; — : PR EoS.

In Figure 28, the comparison is depicted for lower temperatures: filled circles represent the vapor compositions at VLE conditions measured in this work (Tables 7-8); open circles represent the vapor compositions at S_2VE conditions measured in Ref. [8]; solid lines represent the modeling results. Even if experimental compositions of this work and solid lines are at temperatures slightly different from the ones in Ref. [8] (212.59 K, 230.20 K, 242.97 K, and 253.34 K versus 210 K, 230 K, 240 K, and 250 K), it clearly appears that the vapor compositions at S_2VE of Ref. [8] can be seen as an extension of the VLE presented in this work in the low-pressure region at the different temperatures.

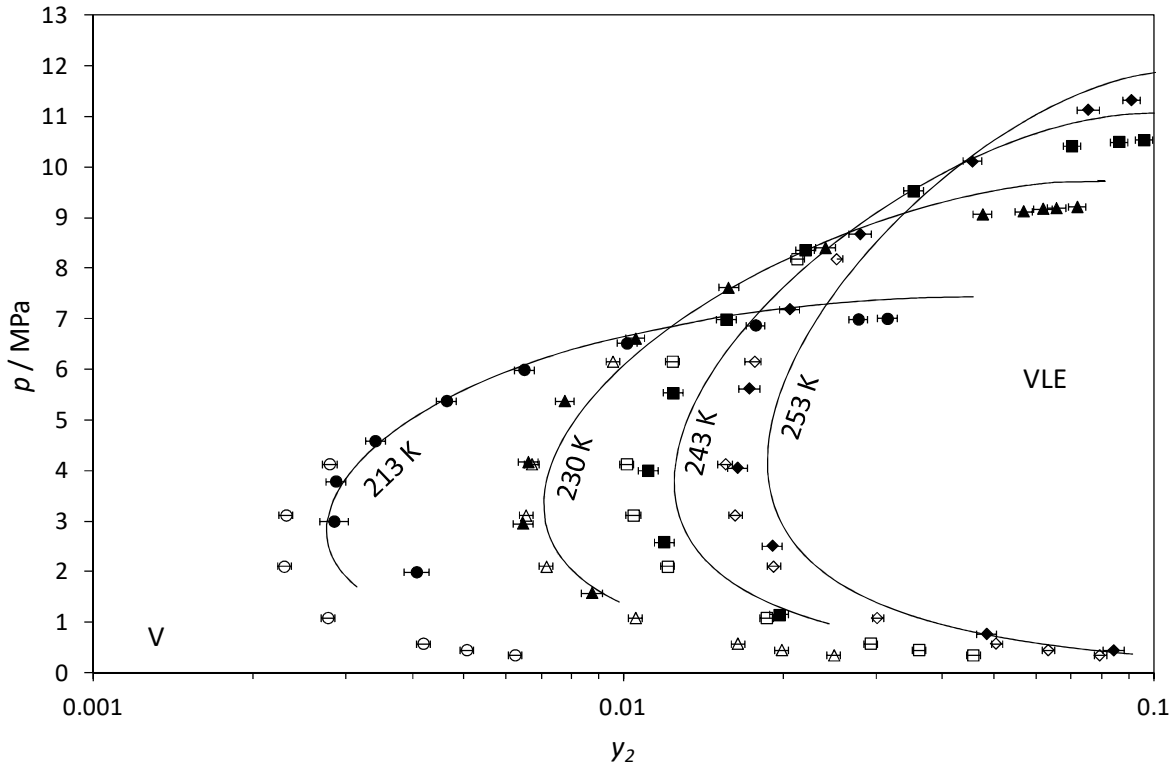

Figure 28. Vapor composition of the (1)CH_4+(2)neo-C_5H_{12} system from 213 K up to 253 K.

Vapor compositions at VLE at 212.59 K (●), 230.20 K (▲), 242.97 K (■), and 253.34 K (♦), this work. Vapor compositions at S_2VE at 210 K (○), 230 K (Δ), 240 K (□), and 250 K (◊), Ref. [8]; — : PR EoS.

To provide an explanation of this behavior, the data of Ref. [8] have been plotted in the pressure-temperature phase equilibrium diagram, Figure 29. All the lines in Figure 29 have been calculated by means of the PR EoS (with k_{ij} from Eq. (19)) and the Classical Approach (for solid neo-pentane in the α,β forms, Eq. (5)-(6)), whereas open circles represent the pressure-temperature coordinates of the S_2VE data of Ref. [8]. Among the low-temperature S_2VE data of Ref. [8] (T < 256.6 K), some of the open circles are located above the $S_{2,\alpha}$LVE line. Provided that the predicted $S_{2,\alpha}$LVE line agrees with the real phase equilibrium behavior of the methane+neo-pentane system, this means that some of the values given in Ref. [8] do not correspond to equilibria between a methane-rich vapor phase and solid neo-pentane.

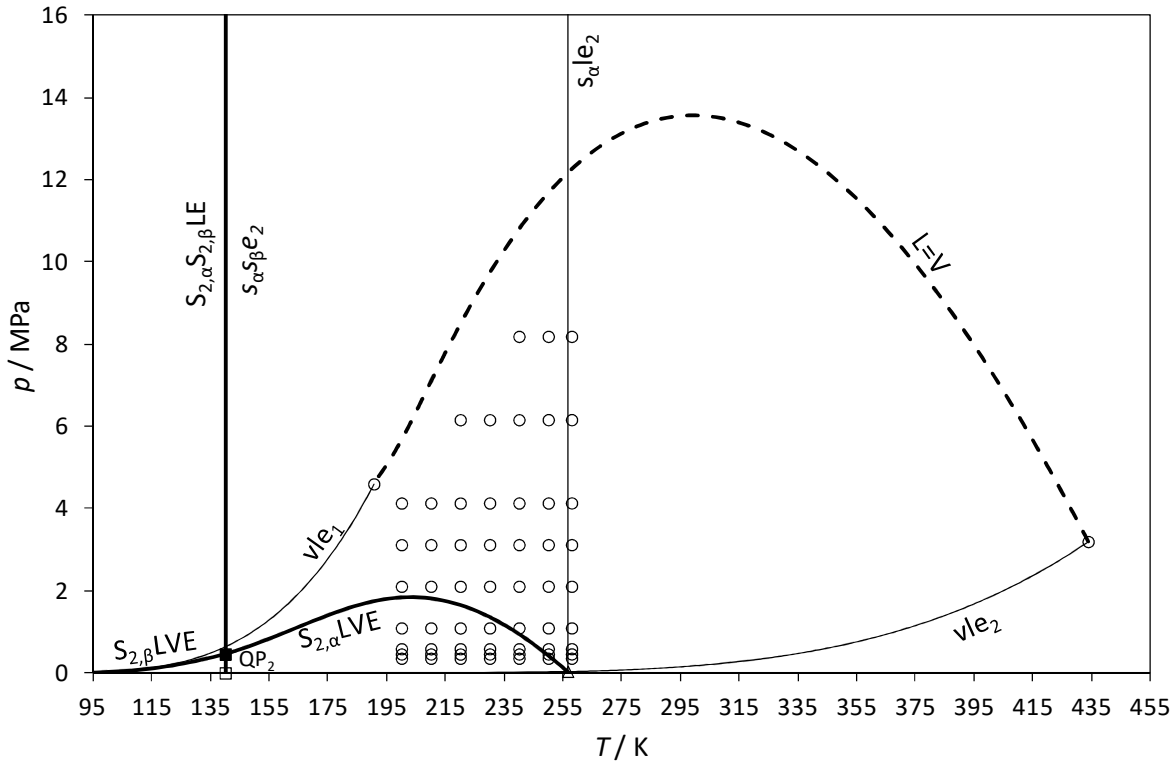

Figure 29. Calculated global phase diagram of the (1)CH_4+(2)neo-C_5H_{12} system down to 95 K.

Pure component properties: — : saturation, melting, sublimation, and solid-solid transition lines; Δ : solid-liquid-vapor triple point; □ : solid-solid-vapor triple point of neo-pentane.
Mixture properties: ▬ : 3-phase equilibrium lines; ■ : QP_1 ($S_1S_{2\beta}$LVE) and QP_2 ($S_{2\alpha}S_{2\beta}$LVE); ▬ ▬ : critical line.
Subscripts: 1 : related to methane; 2 : related to neo-pentane.
S_2VE Ref. [8], (○). Solid-phase model: Classical Approach. Fluid-phase model: PR EoS.

To illustrate, Figure 30 shows the comparison between the pressure-composition phase diagram of the binary system at 230 K as calculated by the PR EoS coupled with the Classical Approach, the VLE presented in this work at 230.20 K, and the data of Ref. [8] at 230 K. The VLE presented in Table 7 are all located at pressures higher than the calculated triple-point pressure (1.35 MPa). To the contrary, 4 equilibrium points at 230 K of Ref. [8] out of 8 are located at pressures lower than the calculated triple-point pressure. The 4 vapor compositions at higher pressures are again well predicted by the PR EoS and agree with the vapor compositions presented in this work. Since that this behavior applies also for the remaining low-temperature S_2VE data of Ref. [8], it can be concluded that a part of these data are representative of VLE conditions rather than S_2VE.

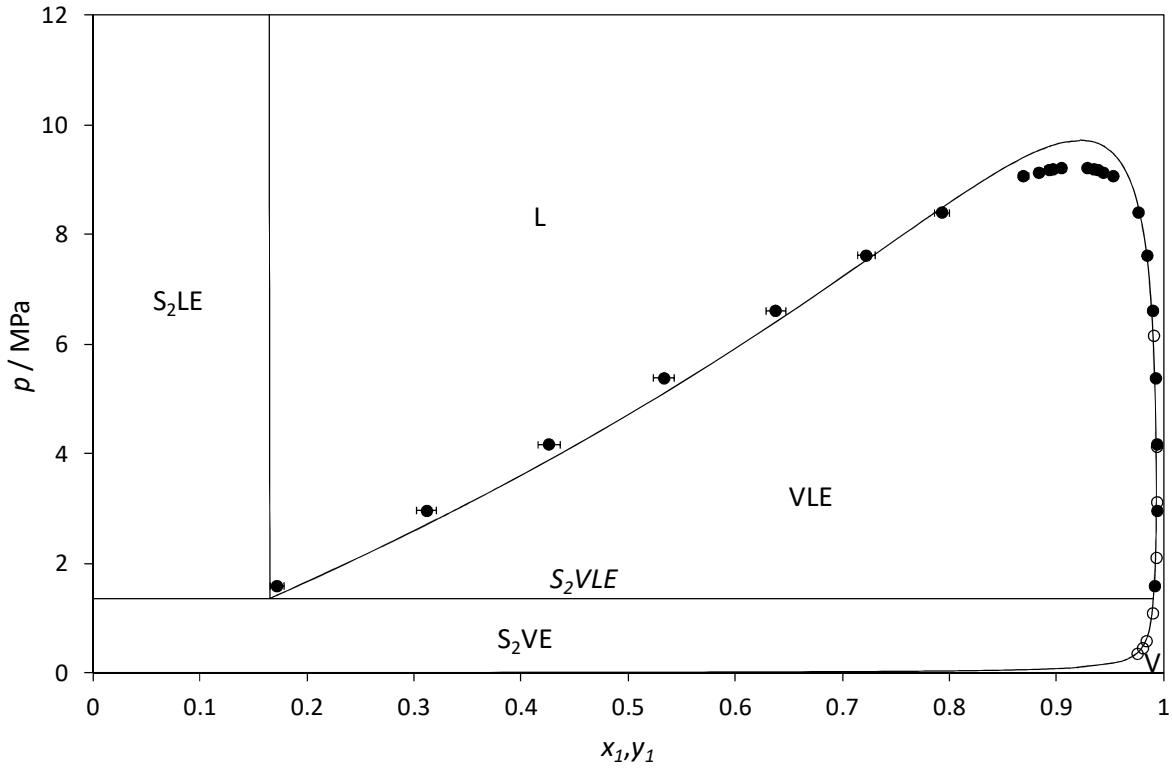

Figure 30. Pressure-composition phase equilibrium behavior at 230 K for the (1)CH_4+(2)neo-C_5H_{12} system.
S_2VE, Ref. [8] (○). VLE, this work (●).
Solid-phase model: Classical Approach. Fluid-phase model: PR EoS.

To end the analysis of the global phase equilibrium behavior of the methane+neo-pentane system:

- The solubility of neo-pentane in vapor and liquid phases along the $S_{2,\alpha}$LVE and $S_{2,\beta}$LVE lines down to 95 K is illustrated in Figure 31.

  In Figure 31, the calculated solubility of solid neo-pentane in the liquid phase (bold continuous line) linearly decreases with decreasing temperatures down to the solid$_\alpha$-solid$_\beta$ transition temperature (140 K), and it is compared with the data of Ref. [9]. The model not only overestimates the solubility of neo-pentane in the liquid phase, but provides also a different temperature effect on the variation of the solubility limit of solid neo-pentane (with crystal structure of kind β) in the liquid phase.

In Figure 31, the bold line is also compared to the ideal (activity coefficient of neo-pentane in the liquid phase equal to 1) solubility of neo-pentane in the liquid phase (thin continuous line) calculated by means of Eq. (24).

$$x_2^{id}(T) = exp\left\{\frac{1}{RT}\left[\Delta H_2^{SLE}\left(\frac{T}{T_{t,2}} - 1\right)\right]\right\} \quad , \quad T \geq 140\ K$$
$$x_2^{id}(T) = exp\left\{\frac{1}{RT}\left[\Delta H_2^{SLE}\left(\frac{T}{T_{t,2}} - 1\right) + \Delta H_2^{SSE}\left(\frac{T}{T_{2,ss}} - 1\right)\right]\right\} \quad , \quad T \leq 140\ K \tag{24}$$

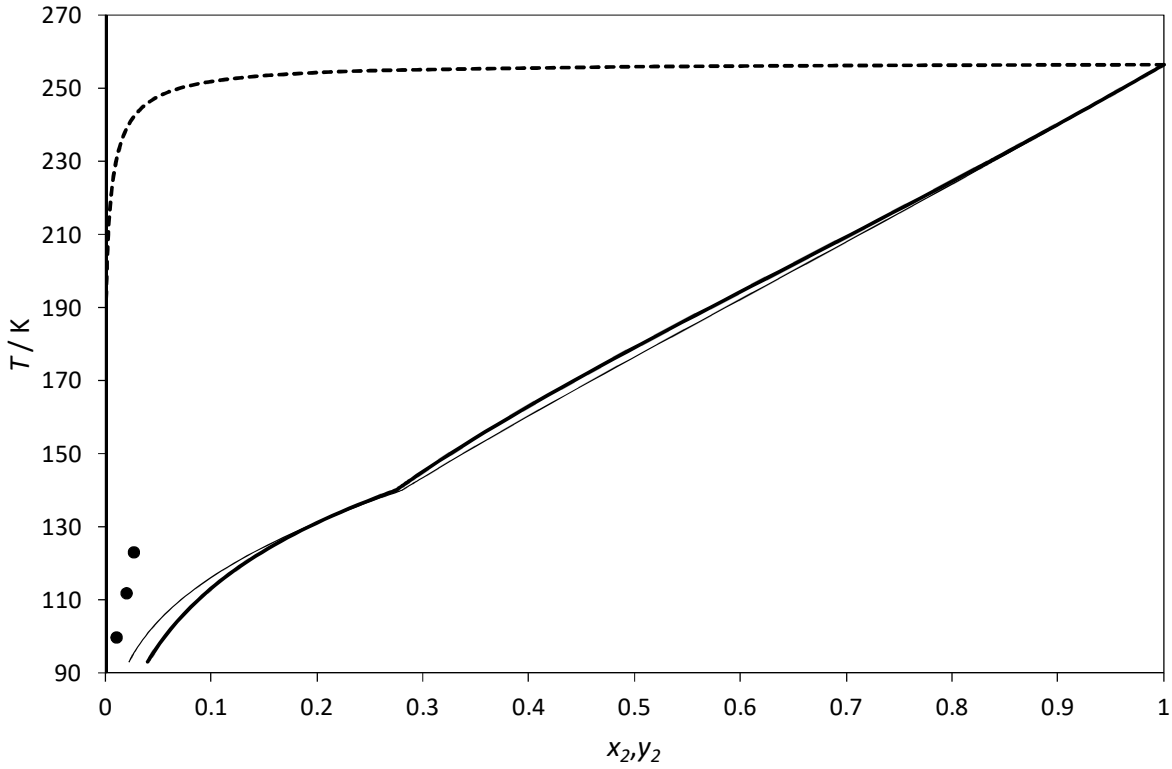

Figure 31. Solubility of neo-C_5H_{12} in the vapor and liquid phase at the $S_{2,\alpha}$VLE and $S_{2,\beta}$VLE of the (1)CH_4+(2)neo-C_5H_{12} system down to 95 K.
S_2LE, Ref. [9] (●); PR EoS + Classical Approach: liquid phase (▬); vapor phase (▬ ▬). Ideal solubility in the liquid phase, Eq. (43): liquid phase (—).

- The calculated critical locus of the mixture is shown in Figure 32 and compared with values calculated by means of the extended scaling laws proposed in Ref. [21]. The calculated critical line is a continuous line joining the critical points of the two pure components, confirming that the fluid-phase equilibrium behavior of the methane+neo-

pentane could be classified as of type I according to the classification of van Konynenburg and Scott.

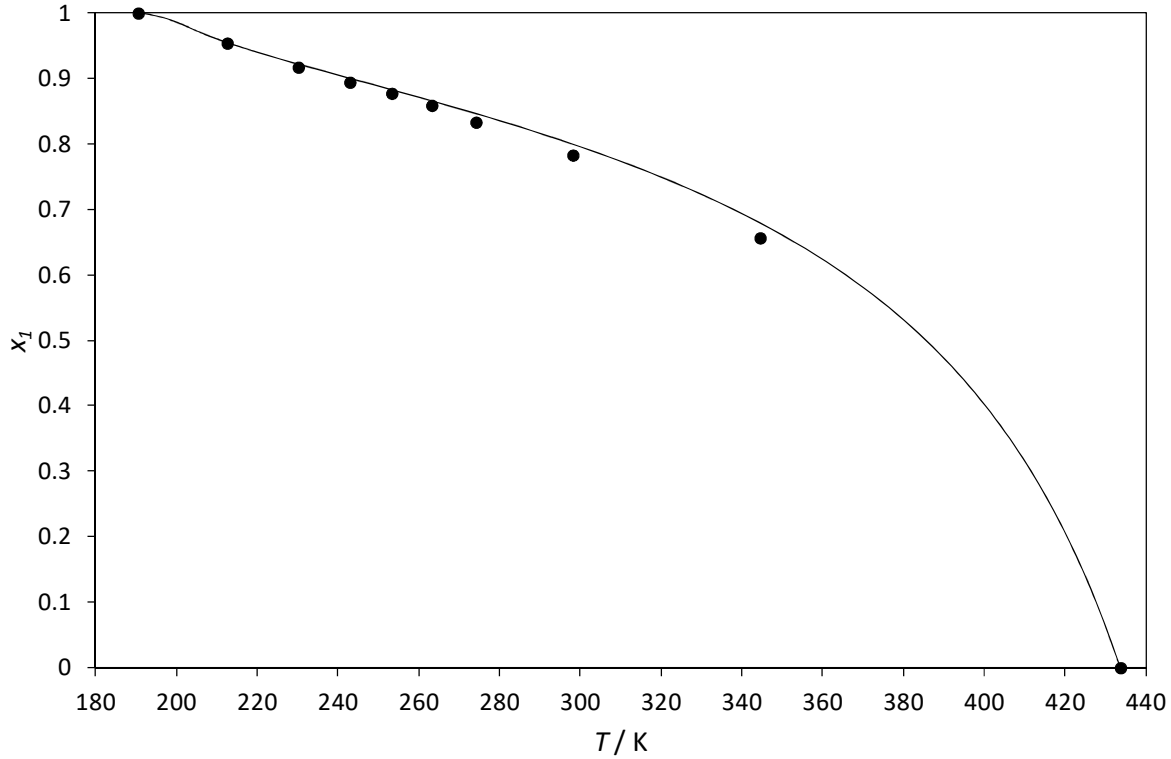

Figure 32. Critical behavior of the (1)CH_4+(2)neo-C_5H_{12} system.
— : PR EoS; Values calculated via the extended scaling laws (●).

6. Conclusions

Similarly to previous investigations of low-temperature phase equilibria and global phase diagrams of binary mixtures of methane, as the one presented in Ref. [26], this research sought to investigate the global phase equilibrium behavior of the methane+neo-pentane system. Original vapor-liquid equilibrium values down to 213 K have been measured by means of a static-analytic apparatus and compared to literature vapor-liquid and solid-vapor equilibrium values.

In the high-temperature region ($T > 256.6$ K), the measured VLE only partially agree with literature values in the temperature range $298 \text{ K} < T < 345$ K, from the quantitative point of view. In the low-temperature region ($T < 256.6$ K), the measured vapor compositions at VLE agree with the literature values at solid-vapor equilibrium down to 210 K.

The new experimental values have been used to obtain a temperature-dependent function for the binary interaction parameter of the methane+neo-pentane system to be used in the Peng-Robinson equation of state. In the temperature range of interest in this work, the binary interaction parameter has been found to be close to zero, providing further insights about the behavior of this mixture of two symmetric, non-polar, and size-different molecules.

The PR EoS has been then coupled with the Classical Approach to predict the global phase equilibrium behavior of the mixture involving solid neo-pentane down to 95 K.

In light of the experimental evidence and the calculated global phase equilibrium behavior, the fluid-phase equilibrium behavior of type III (van Konynenburg and Scott's classification) has been discarded in favor of type I. Contrarily to conclusions that can be drawn from existing literature data (a liquid phase does not exist for temperature between the critical-point temperature of methane and the triple-point temperature of neo-pentane), the VLE data presented in this work confirm that it is possible to maintain methane+neo-pentane mixtures in the liquid state at temperatures much lower than those previously assumed. Furthermore, a

miscibility gap in the liquid phase (liquid-liquid demixing) does not seem to occur in the methane+neo-pentane system, suggesting a global phase equilibrium behavior of type D according to the Kohn and Luks' classification. This conclusion is moreover supported by the experimental analysis carried out by Davenport in 1964, who classified the phase behavior of the methane+neo-pentane system as "completely miscible" since no liquid-liquid demixing was detected by visual observation of three mixtures (25.9%, 41.8%, and 70.6% of neo-pentane on mass basis) between 113 K and 200 K, [25].

In spite of a high value of the triple-point temperature, the predicted solubility limits of the two crystal structures of neo-pentane in liquid methane reveal a high degree of solubility which reduces the risk of solidification of neo-pentane in the natural gas liquefaction process. It remains to be seen if the predicted solubilities at cryogenic temperatures agree with the real behavior of the mixture, and if additional vapor-liquid equilibrium measurements could be performed to validate the proposed functional form of the binary interaction parameters and elucidate the phase equilibrium behavior at temperatures approaching the critical-point temperature of neo-pentane.

Another aspect of particular interest is the purity of the solid phases. The predicted solubilities of neo-pentane in the liquid and vapor phases have been calculated by considering the Classical Approach and total immiscibility in the solid state, which means pure solid phases. The predicted solubilities and solid-fluid equilibrium conditions are in disagreement with literature solid-liquid equilibrium values, thus a deeper investigation should be carried out in the future to confirm the predicted behavior or, to the contrary, to determine if the system is characterized by a solid-fluid equilibrium of the solid-solution type (both methane and neo-pentane molecules participate in the crystal structure of the solid phases, like the methane+krypton system, [27]).

Acknowledgement

This work has been realized in the framework of the ongoing Joint Industry Project "Evaluation of the crystallization risk in LNG production" funded by SHELL, ENGIE, and LINDE.

References

[1] E.W. Lemmon, R. Span, Short fundamental equations of state for 20 industrial fluids, J. Chem. Eng. Data 51 (2006) 785–850. https://doi.org/10.1021/je050186n.

[2] J.S. Chickos, Jr W.E. Acree, J. Liebman, Estimating solid–liquid phase change enthalpies and entropies, J. Phys. Chem. Ref. Data 28 (1999) 1535–1673. https://doi.org/10.1063/1.556045.

[3] U. Setzmann, W. Wagner, A new equation of state and tables of thermodynamic properties for methane covering the range from the melting line to 625 K at pressures up to 1000 MPa, J. Phys. Chem. Ref. Data 20 (1991) 1061–1151. https://doi.org/10.1063/1.555898.

[4] The DIPPR Information and Data Evaluation Manager for the Design Institute for Physical Properties, DIADEM Professional Version 8.0.2, 2016.

[5] P. Stringari, M. Campestrini, S. Hoceini, D. Atig, Gibbs free energy equation of state for solid methane from 21 to 300 K and up to 5000 MPa, J.Chem.Eng.Data, 66 (2021) 1157−1171. https://doi.org/10.1021/acs.jced.0c00960.

[6] N.W. Prodany, B. Williams, Vapor-liquid equilibria in methane-hydrocarbon systems, J. Chem. Eng. Data, 16 (1971) 1–6. https://doi.org/10.1021/je60048a015.

[7] B.L. Rogers, J.M. Prausnitz. High pressure vapor-liquid equilibria for argon+neopentane and methane+neopentane, J. Chem. Thermodynamics, 3 (1971) 221–216. https://doi.org/10.1016/S0021-9614(71)80104-0.

[8] G.L. Baughman, S.P. Westhoff, S. Dincer, D.D. Duston, A.J. Kidnay, The solid+vapor phase equilibrium and the interaction second virial coefficients for argon+, nitrogen+,

methane+, and helium+neopentane; I. Experimental, J. Chem. Thermodynamics, 6 (1974) 1121–1132. https://doi.org/10.1016/0021-9614(74)90148-7.

[9] G.T. Preston, E.W. Funk, J.M. Prausnitz, Solubilities of hydrocarbons and carbon dioxide in liquid methane and liquid argon, J. Phys. Chem., 75 (1971) 2345–2352. https://doi.org/10.1021/j100684a020.

[10] O. Kunz, W. Wagner, The GERG-2008 wide range equation of state for natural gases and other mixtures: an expansion of GERG-2004, J. Chem. Eng. Data, 57 (2012) 3032–3091. https://doi.org/10.1021/je300655b.

[11] E.W. Lemmon, I.H. Bell, M.L. Huber, M.O. McLinden, NIST Standard Reference Database 23, Reference Fluid Thermodynamic and Transport Properties - REFPROP, DLL version number Version 10.0, Applied Chemicals and Materials Division, 2018.

[12] P.H. van Konynenburg, R.L. Scott, Critical lines and phase equilibria in binary van der Waals mixtures, Phil. Trans. R. Soc. Lond., 298 (1980) 495–540. https://doi.org/10.1098/rsta.1980.0266.

[13] J.P. Kohn, K.D. Luks, Solubility of hydrocarbons in cryogenic LNG and NGL mixtures, Gas Processor Association, Research Report 22, 1976.

[14] J.N. Jaubert, F. Mutelet, VLE predictions with the Peng–Robinson equation of state and temperature dependent k_{ij} calculated through a group contribution method, Fluid Phase Equilib., 224 (2004) 285–304. https://doi.org/10.1016/j.fluid.2004.06.059.

[15] T. Holderbaum, J. Gmehling, PSRK: A group contribution equation of state based on UNIFAC.,Fluid Phase Equilib., 70 (1991) 251–265. https://doi.org/10.1016/0378-3812(91)85038-V.

[16] J.P. Prausnitz, R.N. Lichtenthaler, E.G. de Azevedo, Molecular thermodynamics of fluid-phase equilibria, second ed., Prentice-Hall, Englewood Cliffs, NJ, 1986.

[17] Simulis Thermodynamics, version 2.0.4, ProSim SA, Lab_ege, France.

[18] E. Boonaert, A. Valtz, J. Brocus, C. Coquelet, Y. Beucher, F. De Carlan, J.-M. Fourmigué , Vapor-liquid equilibrium measurements for 5 binary mixtures involving HFO-1336mzz(E) at temperatures from 313 to 353 K and pressures up to 2.735 MPa, Int. J. Refrigeration, 114 (2020) 210–220. https://doi.org/10.1016/j.ijrefrig.2020.02.016.

[19] P. Guilbot, A. Valtz, H. Legendre, D. Richon, Rapid on-line sampler-injector: a reliable tool for HT-HP sampling and on-line GC analysis, Analusis 28 (2000) 426–431. https://doi.org/10.1051/analusis:2000128.

[20] B.N. Taylor, C.E. Kuyatt, Guidelines for evaluating and expressing the uncertainty of NIST measurement results., Technical report, National Institute of Standards and Technology, Gaithersburg, MD, 1994.

[21] P. Ungerer, B. Tavitian, A. Boutin, Applications of molecular simulation in the oil and gas industry- Monte Carlo Methods, IFP Publications, Paris, France, 2005.

[22] D.-Y. Peng, D.B. Robinson, A new two constant equation of state, Ind. Eng. Chem. Fundament., 15 (1976) 59–64. https://doi.org/10.1021/i160057a011.

[25] J. Davenport, Thermodynamics of solutions in liquid methane, Imperial College of Science and Technology, London, Ph.D. Thesis, 1964.

[26] M. Campestrini, P. Stringari, Solubilities of solid n-alkanes in methane: data analysis and models assessment, AIChE J., 64 (2018) 2219–2239. https://doi.org/10.1002/aic.16071.

[27] M. Von Stackelberg, F. Quatram, H.J. Antweiler, Mischkristalle von methan und krypton, Z. Elektrochem., 42 (1936) 552–557.